


RESEARCH

Open Access



ITIH5-mediated fibroblast/macrophage crosstalk exacerbates cardiac remodelling after myocardial infarction

Yirong Wu^{1†}, Li Meng^{1,3†}, Siyao Zhan¹, Miaofu Li¹, Jiamin Huang^{1,3}, Xuechun Chen¹, Liuying Chen¹, Xiaofei Gao¹, Hao Chen^{1,3}, Huimin Chen^{1,3}, Yigang Zhong^{1*}, Linhao Xu^{1,2*} and Yizhou Xu^{1,3*} 

Abstract

Background Myocardial infarction (MI) and subsequent ischaemic cardiomyopathy (ICM) are the primary causes of heart failure. Inter- α trypsin inhibitor heavy chain 5 (ITIH5) is an extracellular matrix (ECM) protein and has been identified as a myocardial marker of ICM. However, its diagnostic value in patients with ICM and its function and molecular mechanism in regulating cardiac repair and remodelling after MI remain unknown.

Methods Three microarray datasets including 117 ICM and 152 non-failing (NF) myocardial tissue samples were merged and analysed. Peripheral blood and clinical information were collected from 53 patients with ICM and 40 NF controls. The effects of ITIH5 on cellular interactions and cardiac remodelling was studied using ITIH5 RNAi adenovirus and mouse MI model in vivo and in fibroblast–macrophage co-culture model in vitro.

Results ITIH5 was upregulated in the myocardial tissue and peripheral blood of patients with ICM and could be an independent risk factor for ICM. Experiments in mice suggested that ITIH5 promotes cardiac fibrotic remodelling at all phases after MI. Downregulation of ITIH5 increased the risk of death within 7 d after MI but inhibited ventricular remodelling and improved cardiac function on the long-term. ITIH5 promotes the primary cardiac fibroblasts (CFs) proliferation, migration, and improves survival rather than activation. Moreover, ITIH5 directly promotes macrophage tissue infiltration, maturation, and profibrotic phenotype transformation, thereby promoting fibrotic remodelling. By using fibroblast–macrophage co-culture model, we demonstrated ITIH5 enhanced the fibroblast/macrophage cross-talk manifest as macrophage profibrotic phenotype transformation and CFs activation, mainly by enhancing the hyaluronan stability, the ability of ITIH5 to bind macrophage CD44 receptors and the downstream activation of the signal transduction and activator of transcription 3 pathway in macrophages.

Conclusions ITIH5 could be used as a diagnostic marker for ICM. Moreover, ITIH5 expression was upregulated after MI, which accelerated ECM-fibroblast-macrophage interaction, thereby promoting macrophage profibrotic phenotype transformation, CFs activation, and cardiac fibrotic remodelling.

Keywords Myocardial infarction, Ischaemic cardiomyopathy, ITIH5, Extracellular matrix, Cell–cell communication

[†]Yirong Wu and Li Meng have contributed equally to this work.

*Correspondence:

Yigang Zhong

hzsyxkzyg@163.com

Linhao Xu

xulinhaoluck@163.com

Yizhou Xu

xuyizhouzju@163.com

Full list of author information is available at the end of the article



© The Author(s) 2025. **Open Access** This article is licensed under a Creative Commons Attribution-NonCommercial-NoDerivatives 4.0 International License, which permits any non-commercial use, sharing, distribution and reproduction in any medium or format, as long as you give appropriate credit to the original author(s) and the source, provide a link to the Creative Commons licence, and indicate if you modified the licensed material. You do not have permission under this licence to share adapted material derived from this article or parts of it. The images or other third party material in this article are included in the article's Creative Commons licence, unless indicated otherwise in a credit line to the material. If material is not included in the article's Creative Commons licence and your intended use is not permitted by statutory regulation or exceeds the permitted use, you will need to obtain permission directly from the copyright holder. To view a copy of this licence, visit <http://creativecommons.org/licenses/by-nc-nd/4.0/>.

Background

Myocardial infarction (MI) is a leading cause of heart failure worldwide. Cardiac ischaemia and hypoxia lead to localised or diffuse myocardial fibrosis, which in turn lead to impaired systolic and/or diastolic function of the heart and development of ischaemic cardiomyopathy (ICM) [1, 2]. The body adapts to MI injury through complex acute and chronic responses to maintain the pump function; this process is mediated with inflammation and immune cell signalling [3].

In acute ischaemic injury, immune-mediated fibrotic activation is necessary to prevent catastrophic myocardial rupture. Substitutional fibrosis in the infarct area results from the activation of interstitial fibroblasts and recruitment of epicardial fibroblasts, leading to scar formation and maintenance of ventricular integrity. However, an excessive fibroblast response leads to the accumulation of excessive extracellular matrix (ECM), which stiffens the cardiac tissue and negatively affects the niches of cardiomyocytes, leading to the progressive deterioration of cardiac function [4, 5]. Although fibroblast activation has been extensively studied, the effects of immune signalling on acute and chronic fibrosis have recently received widespread attention [4, 6]. The understanding of this relationship will revolutionise the treatment of heart diseases by targeting the immune regulation. Although the development of chimeric antigen receptor T-cell immunotherapy offers exciting future directions [7, 8], there is currently a lack of specific immune regulatory targets for heart failure after MI and further exploration is needed.

Matricellular proteins are non-structural ECM proteins that interact with cell surface receptors, growth factors, proteases, and other bioactive substances, as well as with ECM structural proteins [9, 10]. Therefore, matricellular proteins acts as the "bridge" of information exchange between cells and ECM, and are involved in maintaining the integrity of cardiac structure and regulating the immune environment after MI, a key factor that determines prognosis [10, 11]. Inter- α trypsin inhibitor heavy chain 5 (ITIH5) can be secreted into ECM and has been widely reported as a tumour suppressor gene [12–15]. Recent studies have identified ITIH5 as a potential adipokine, and its expression in the abdominal subcutaneous adipose tissue of patients with obesity is higher than that in the patients who are non-obese [16, 17]. In addition, some studies have revealed a role of ITIH5 in regulating ECM and immune environmental homeostasis. First, ITIH5 regulates the myofibroblast trans-differentiation and activation of the endothelin-dependent transforming growth factor beta (TGF β) signalling pathway [18, 19]. ITIH5 knockout promotes periostin and multiple matrix metalloproteinases expression in inflammatory skin disease models [20]. In contrast, ITIH5 is a

potential immune cell regulator that maintains high-density hyaluronan (HA) and prevents its degradation into pro-inflammatory low-density HA, thereby improving a variety of inflammatory skin diseases [20, 21] and inhibiting pro-inflammatory cytokine synthesis in adipose stem cells [22].

Previous studies have identified ITIH5 as a myocardial marker of ICM and its association with chronic kidney disease [23]; however, there is still a lack of evidence on the diagnostic value of ITIH5 in patients with ICM and its function and molecular mechanism in regulating tissue repair and remodelling after MI. In this study, by integrating gene microarray datasets and detecting ITIH5 levels in the peripheral blood, we found that both myocardial and peripheral blood ITIH5 levels could be used as diagnostic markers of ICM. Further, we used an adeno-associated virus (AAV) system to knockdown the ITIH5 gene in vivo and a fibroblast/macrophage 2/3D co-culture model in vitro, to study ITIH5-mediated cardiac remodelling and ECM–macrophage–fibroblast signalling network regulation after MI. We explored the molecular mechanism by which ITIH5 regulates ECM structure and downstream signalling pathways, which could promote macrophage profibrotic phenotypic transformation. In this study, we identified novel diagnostic markers of ICM, revealed a new mechanism of ECM regulation of cardiac remodelling after MI, and provided new clues for the treatment of MI and ICM.

Materials and methods

Reagents and antibodies

The signal transduction and activator of transcription 3 (STAT3) inhibitor (Stattic, HY-13818) and 4-methylumbelliferone (4-MU, HY-N0187) were purchased from MedChemExpress (New Jersey, USA). The anti-mouse/human CD44 neutralizing antibody (BE0039) and IgG2b isotype control (BE0090) were purchased from BioXcell (West Lebanon, USA). The primary antibodies anti-CD44 (15675–1-AP), anti-STAT3 (10253–2-AP), anti- β -actin (20536–1-AP), anti-GAPDH (10494–1-AP), anti-collagen I (14695–1-AP), anti-collagen III(68320–1-Ig), anti- α SMA (14395–1-AP), anti-CtlnI (21652–1-AP), anti-CD31 (28083–1-AP), anti-F4/80 (28463–1-AP), anti-CD3 (17617–1-AP), anti-CD68 (28058–1-AP), anti-CSF1R (25949–1-AP), anti-iNOS (18985–1-AP) anti-CD86 (13395–1-AP), anti-ARG1 (66129–1-Ig), anti-CD206 (60143–1-Ig) and anti-TGF β 1 (21898–1-AP) were purchased from Proteintech (Wuhan, China). Anti-OPN (ab91655) was purchased from Abcam (Cambridge, UK). Anti-Ki67 (HA721115) and anti-phospho-STAT3 Tyr705 (ET1603-40) were purchased from HUABIO (Hangzhou, China). Anti-BAX (2772), anti-caspase 3 (14220),

anti-vimentin (5741), and anti-LY6G (87048) were purchased from Cell Signaling Technology (Danvers, MA, USA). Anti-ITIH5 (OACD04924) was purchased from Aviva systems biology (San Diego, CA, USA).

Data collection and processing

Using the keywords “ischemic cardiomyopathy”, we downloaded three microarray expression profiles of human ischaemic cardiomyopathy from the Gene Expression Omnibus (GEO) database (<https://www.ncbi.nlm.nih.gov/geo/>), including the GSE42955, GSE79962, and GSE57338 datasets. The platform for GSE42955 and GSE79962 was GPL6244, which included 23 ICM samples and 16 non-failing (NF) donor heart samples. The platform for GSE57338 was GPL11532 which included 95 ICM samples and 136 NF donor heart samples.

The R software package was used to process the downloaded platform and a series of expression matrix files. The ID corresponding to the probe name was converted to the international standard name for the genes (gene symbols) by using “hugene10sttranscriptcluster.db” and “hugene11sttranscriptcluster.db” R packages respectively. We combined the three datasets because the GPL6244 and GPL11532 platforms shared the same probe to the gene symbol conversion annotation information. After merging all the microarray data, batch effects were adjusted by the “combat” function of the “sva” package. Finally, the expression values were normalised according to the “normalizeBetweenArrays” function of the package “limma” so that the expression values have similar distribution across a set of arrays.

In addition, another human ICM microarray expression profile (GSE5406) and an RNA sequencing expression profile (GSE116250) were downloaded as external validation datasets to verify the differential expression tendency of ITIH5. The ID corresponding to the probe name in GSE5406 dataset was converted to gene symbols by using “hgu133a.db” R package and the Ensembl ID in GSE116250 dataset was converted to gene symbols by using “biomart” R package. Information on the five datasets is listed in Additional file 1 (Table S1).

Screening for DEGs

We screened the differentially expressed genes (DEGs) between the patients with ICM and NF heart in the merged data using the “limma” R package. A gene was defined as a DEG between the ICM and NF samples when the adjusted *P* value was < 0.05 and $|\log_2 \text{FC}| > 0.6$.

Identification of hub genes

Hub genes were identified using the weighted gene co-expression network analysis (WGCNA) R package and

the correlation coefficients of the genes were constructed and transformed into a weighted adjacency matrix. These genes were then allocated to minimum-sized modules, and a cluster dendrogram was drawn. A total of 20 genes was chosen as the minimum number of genes in each module. To merge possible similar modules, we defined 0.2 as the threshold for cut height. The correlation between gene expression and sample trait was determined by the criterion of gene significance > 0.5 and module membership > 0.83 .

Random forest analysis

The random forest package was used to analyse the intersecting genes. Random forest is one of the most widely used machine learning algorithms; it can process input samples with high-dimensional features without dimensionality reduction and evaluate the importance of each feature in classification problems.

Single cell sequencing data collection and processing

Using the keyword “Myocardial infarction”, we downloaded a mice single cell sequencing dataset GSE128628 from the GEO database (<https://www.ncbi.nlm.nih.gov/geo/>). The datasets included one left ventricular myocardial tissue sample from the sham operation group and two left ventricular myocardial tissue samples from the MI model group two weeks after MI modelling. The Seurat (version 4.0, <https://satijalab.org/seurat/>) R package was used for raw scRNA-seq data processing and preliminary analysis. The details are as follows:

- (1) Seurat was used to convert the scRNA-seq data into Seurat objects.
- (2) Seurat was used to screen high-quality cells based on the criteria that the number of expressed genes was less than 200 and that the proportion of mitochondrial genes was more than 20%. If one of these criteria was satisfied, the cells were filtered.
- (3) The “harmony” function was used to remove the batch effect and standardise the data.
- (4) The first 3,000 highly variable genes were determined using the “FindVariableFeatures” function, and then principal component analysis was applied to reduce the dimensionality of the scRNA-seq data based on 3,000 variable genes.
- (5) The “RunTSNE” function was applied to perform t-distributed stochastic neighbour embedding (TSNE) to analyse the scRNA-seq data. Cell cluster analysis was conducted by the “FindClusters” function (with the “resolution” parameter set to 0.6) and the “FindAllMarkers” function was used to identify DEGs between each cell population.

(6) Finally, different cell populations were annotated according to the marker genes obtained from the “CellMarker” database and previous studies [24, 25].

RNA sequencing and bioinformatic analysis

A small portion of fresh myocardium of the infarction area (approximately 5–10 mg) from three hearts in each of the groups was used to extract total RNA. The mRNA-seq Library Prep kit (Vazyme, Nanjing, China, cat#NR612-02) was used to prepare a transcriptome library with at least 1 µg total RNA. Transcriptome sequencing and analysis were conducted by OE Biotech Co. Ltd. (Shanghai, China). Differential expression analysis was performed using the R package ‘DESeq2’. The thresholds for significant DEGs were set as $p < 0.05$ and \log_2 fold change (FC) values > 1 or < -1 . GO enrichment, KEGG pathway enrichment and GSEA enrichment analyses of DEGs were performed using the Xiantao platform (<https://www.xiantao.love/products>).

Collection, acquisition, and processing of clinical samples

Peripheral blood samples were obtained from 40 volunteers without heart failure and 53 patients with ICM at the Cardiology Department of Hangzhou First People’s Hospital (Hangzhou, China). The inclusion criteria were as follows: (1) a clear history of coronary heart disease with at least one MI event, and (2) signs and/or laboratory evidence of cardiac insufficiency. The healthy control population included relatively healthy volunteers with no history of heart failure or coronary heart disease but had cardiovascular disease risk factors. The exclusion criteria were as follows: (1) patients with other heart diseases or other causes of heart enlargement and heart failure, including dilated cardiomyopathy, congenital cardiovascular disease, pulmonary heart disease, valvular heart disease, and other cardiomyopathies due to various secondary causes, such as rapid and persistent supraventricular arrhythmia; (2) patients with severe hepatic and renal insufficiency; (3) patients with severe infections; and (4) patients with malignant tumours. This study followed the ethical standards formulated by the Declaration of Helsinki of the World Health Organization and was approved by the Ethics Committee of Hangzhou First People’s Hospital (Research KY-20230827–0187–01). All samples were centrifuged at 3,000 rpm and 4 °C for 10 min within 12 h after collection. Peripheral blood plasma for enzyme-linked immunosorbent assay (ELISA) tests was collected and stored at -80 °C.

Animal experiments

C57BL/6 male mice, aged 5–6 weeks old and weighing 18–20 g, were provided by the Zhejiang Chinese Medical University. Animal experiments were conducted at the Experimental Animal Center of Zhejiang Chinese Medical University under the registration number IACUC-20230710–07 (approval July 2023). The mice were housed in a specific pathogen-free facility, maintained at 22 °C with 12 h of light per day, and provided ad libitum access to food and water. After allowing the mice to acclimatise for 7 d, they were randomly assigned to the experimental groups.

AAVs preparation and mice tail vein injection

After adaptive feeding for one week, tail vein injections of AAVs were performed. The mice in the WT group received a tail vein injection of 100 µL 5.0×10^{11} vg AAV9-pPOSTN-scramble; the mice in the ITIH5 knockdown (KD) group received a tail vein injection of 100 µL 5.0×10^{11} vg AAV9-pPOSTN-shITIH5. The AAVs used in this study were purchased and synthesised by Shanghai Genechem Co., Ltd. (Shanghai, China).

Mice MI model construction

The mice were fed for three weeks after tail vein injection, and a mouse MI model was constructed. Each group of mice was randomly divided into two groups for MI construction and sham operations, the specific steps are as follows:

- (1) The mice were weighed, and the surgical site was fully exposed after intraperitoneal injection of pentobarbital sodium (50 mg/kg).
- (2) Subsequently, the mice were placed in the supine position, their limbs and teeth were fixed, and a tracheal tube was inserted and connected to a ventilator. The chest fluctuated and moved along with the ventilator, which was set at a suction frequency of 100 times/min and the tidal volume was set to 0.5–0.7 mL.
- (3) The mice were then placed in the right decubitus position, and the chest was opened between the ribs (3–4) and the armpit of the left forelimb to fully expose the heart. A small portion of the pericardium was torn under the left atrial appendage to fully expose the left anterior descending branch.
- (4) The 7–0 sutures with needles were placed with the needle holder and inserted at the lower margin of the left atrial appendage (1.5 mm). The stitches passed through the left anterior descending branch to completely block the blood flow of the left ante-

rior descending branch. The sham operation group was threaded without a ligature.

- (5) After ligation, the 4–0 suture completely closed the chest cavity opening and closed the chest cavity layer-by-layer from the inside to the outside.
- (6) Respiratory support was continued to be administered to the mice after surgery; when the depth of anaesthesia of the mice decreased and spontaneous breathing resumed, tracheal intubation was pulled out and the mice were put back into the cage to recommence normal life. Feeding was continued for 7 or 28 d after construction of the MI model.

Echocardiographic assessment of cardiac functions

Seven or 28 days after the establishment of the MI model, the mice were anaesthetised with isoflurane. The cardiac function of the left ventricle (LV), including LV ejection fraction (LVEF), LV fractional shortening (LVFS), and LV internal dimensions at diastole/systole (LVIDd/LVIDs), was evaluated using echocardiography with a Vevo TM 2100 (Visual Sonics Inc., Ontario, Canada) in the transthoracic parasternal long-axis view.

Histological staining

After echocardiographic and electrophysiological assessments, hearts were isolated and fixed in 4% paraformaldehyde for 24 h, followed by gradual dehydration. Fixed heart tissues were embedded in paraffin and subjected to haematoxylin and eosin (H&E) and Masson's trichrome staining. To label the macrophages and lymphocytes in the heart tissues of mice, antibodies against murine F4/80, LY6G, and CD3 were used for immunohistochemical staining. All the pathological staining and immunohistochemical sections were obtained using a digital slide scanner (Aperio Versa 8; Leica, Germany).

Tissue immunofluorescence and HA detection

Hearts were isolated and fixed in 4% paraformaldehyde for 24 h, followed by gradual dehydration. Fixed heart tissues were embedded in paraffin. The paraffin was removed from the sections with xylene and ethanol using standard procedures. Antigen retrieval was performed using 10 mM citrate buffer, boiling for 20 min, cooling for 20 min, and rinsing with PBS. Slides were permeabilised with 0.5% Tween-20 in PBS for 10 min. Non-specific staining of tissue sections was minimised by blocked with 10% normal goat serum in PBS at room temperature for 60 min. Slides were incubated overnight at 4 °C with primary antibody. Sections were washed with PBS to remove unbound antibodies and then incubated for 60 min at room temperature in the dark with Alexa Fluor 488 (Beyotime), Alexa Fluor 647 (Beyotime), or

streptavidin-FITC (Beyotime). Then DAPI (Beyotime) was used to stain the nucleus after washing the slides with PBS to remove unbound antibody. Images were captured by tissue panoramic scanning microscopy (Pannoramic SCAN, 3D HISTECH, Hungary) or confocal microscope (LSM900, Zeiss, Germany) after the slides were sealed using anti-fluorescence quenching sealing tablets.

Tunel staining

Tissue apoptosis was determined by TUNEL staining. Briefly, brain tissues were excised and fixed in 4% paraformaldehyde in PBS at room temperature for 24 h. The fixed tissues were embedded in paraffin and stained using a TUNEL kit (Roche Diagnostics).

Cell isolation and culture

Bone marrow-derived macrophages (BMDMs) were isolated from 6 to 8 week-old mice the femur and tibia. The bones were flushed with Dulbecco's modified Eagle's medium (DMEM) supplemented with 10% foetal bovine serum FBS (Invitrogen). BMDMs were cultured in DMEM supplemented with 10% FBS (Invitrogen Gibco), 100 U/mL penicillin–streptomycin (Invitrogen Gibco), and 10 ng/L macrophage colony-stimulating hormone (Novoprotein, Suzhou, China; C756) for 6 d.

Primary cardiac fibroblasts (CFs) were isolated from 3 day-old neonatal mice by collagenase type II (Worthington, Lakewood, NJ, USA; LS004177) digestion [24]. Briefly, hearts were excised, minced, and placed in spinner flasks containing 0.1% collagenase type II. The ventricles were repeatedly digested (10–15 min at 37 °C), and the cells released by the second to fifth digestions were pooled, pelleted, and resuspended in DMEM supplemented with 10% FBS (Invitrogen Gibco) and 100 U/mL penicillin–streptomycin (Invitrogen Gibco). The cells were plated for 45 min to allow the CFs to preferentially attach, after which unattached cells were removed by aspiration and fresh medium was added. In this experiment, CFs were sub-cultured using trypsin and used within three passages.

Mouse Raw264.7 cells were obtained from the cell bank of the Chinese Academy of Sciences (Shanghai, China). RAW264.7 cells were cultured in DMEM supplemented with 10% FBS and 100 U/mL penicillin–streptomycin.

Cell lentivirus transfection and stable transfected cell line construction

Lentiviruses carrying the ITIH5 coding sequence and a control virus with a green fluorescent protein tag were purchased from Shanghai Genechem Co., Ltd. (Shanghai, China). The procedure is as follows:

- (1) The day before lentivirus infection, 1×10^5 CFs were seeded in each well of a 6-well plate or 1×10^5 Raw264.7 cells in each well of 24-well plates.
- (2) For Raw264.7 cells infection, the appropriate volume of lentivirus (MOI=100), 20 μ L HiTransG P infection reagent, and DMEM with 10% FBS was configured with a final volume of 500 μ L; for CFs infection, the appropriate volume of lentivirus (MOI=100), 40 μ L HiTransG P infection reagent, and DMEM with 10% FBS was configured with a final volume of 1 mL.
- (3) The original medium in each well was discarded, and mixed medium was added to each well.
- (4) The mixed medium was replaced after 18 h by DMEM containing 10% FBS.
- (5) CFs infected with lentivirus were sub-cultured using trypsin and used for experiments within three passages.
- (6) For stably transfecting Raw264.7 cells, the original medium was replaced with DMEM supplemented with 10% FBS and 10 mg/mL puromycin until the cells reached 50% confluency. The culture was continued until the cell density reached 90% confluency, and then the cells were cultured in DMEM with 10% FBS and 10 mg/mL puromycin for 1 or 2 generations.

CFs and BMDMs siRNA transfection

Approximately 5×10^5 CFs were seeded into the wells of a 6-well plate until the cells reached 70–80% confluency. For BMDMs, were to induce to differentiate using macrophage colony-stimulating factor (M-CSF) for 5–6 days until the cells reached 70–80% confluency. For transfection, the appropriate volume and concentration of si-ITIH5 oligonucleotides (sequence were CAGAACCUCAGACGAUAAUTT and AUUAUCGUCUGAGGUUCU GTT, for sense and antisense sequences, respectively) or that of negative control siRNA (si-NC) were mixed with INTERFERin transfection reagent (Polyplus, Strasbourg, France) and added to 200 μ L Opti-MEM. The mixed transfection agent was vortexed and incubated at room temperature for 10 min. Cells were transfected by replacing the culture medium with Opti-MEM and mixed transfection agent was added to each well. After gentle mixing and culturing in an incubator for 6 h, the medium was replaced with DMEM containing 10% FBS.

Two-dimensional co-culture system construction

After lentivirus transfection of CFs, the medium was discarded, the cells were collected follow trypsinisation for 3 min using 0.25% trypsin. Approximately 2×10^5 CFs were seeded into the wells of 12-well plates. After 24 h, the culture medium was replaced with 10% FBS DMEM

containing 20 ng/mL M-CSF, and approximately 2×10^5 BMDMs/well were added and co-cultured with the CFs. Further treatment was performed after 5–6 d of continuous co-culture.

Three-dimensional spheroid co-culture system construction

After lentivirus infection of CFs, the medium was discarded, and the cells were trypsinised with 0.25% trypsin for 3 min. Approximately 5×10^3 CFs were seeded in each well of a 96-well ultra-low-adsorption spheroid microplate (Corning Inc., Corning, USA). After 24 h, approximately 2000 BMDMs/well were seeded per well and co-cultured with the CFs and the culture medium was replaced by 10% FBS DMEM with 20 ng/mL M-CSF. Further treatment was carried out after 5–6 days of continuous co-culture.

Cells or co-culture system treatment

CFs were treated with 1 μ g/mL angiotensin (MedChem-Express) or kept under hypoxic conditions (94% N₂, 1% O₂, 5% CO₂) for 24 h. CFs were cultured in FBS-free DMEM for 24 h to induce apoptosis. BMDMs were treated with 10 ng/mL interleukin 4 to promote profibrotic phenotype transformation.

For the co-culture system treatment, HA synthesis was inhibited by 4-Methylumbelliferone (4-MU); CD44 binding ability was inhibited by CD44 neutralizing antibody and non-specific isotype control antibody was used as a control. STAT3 phosphorylation was inhibited by the broad-spectrum STAT3 inhibitor Stattic. Following the co-culture of cells for 5–6 days, the medium was changed to DMEM complete medium containing the above-mentioned inhibitors or neutralising antibodies (4-MU 0.5–1 mM, Stattic 1–2 μ M, CD44 neutralising antibodies or non-specific isotype control antibody 5 μ g/mL), and the culture was continued for 24 h.

ELISA

ELISA was used to measure ITIH5 and NT-proBNP in human plasma and mouse serum samples, respectively, using commercial kits according to the manufacturer's instructions. The human ITIH5 ELISA Kit was from Aviva Systems Biology (CA, USA) and the Mouse NT-proBNP ELISA Kit was from Elabscience Biotechnology Co., Ltd.

Quantitative reverse transcription (qRT-PCR)

Total cellular and tissue RNA were isolated using the RNA-Quick Purification Kit and Tissue RNA Purification Kit Plus (Yishan, Shanghai, China), respectively, according to the manufacturer's recommendations. The isolated RNA was quantified using the photometric method with a NanoDrop spectrophotometer (Thermo

Fisher Scientific). Subsequently, 500 ng of total RNA was reverse-transcribed into cDNA using a HiFiScript cDNA synthesis kit (CWbio, Taizhou, China) following the manufacturer's instructions. The qRT-PCR primers used in this study were synthesised by Sangon Biotech (Shanghai, China) and their sequences are shown in Table S2. For qRT-PCR, the UltraSYBR mixture (CWBio) and the ABI Q5 real-time PCR detection system (Thermo Fisher Scientific) were used to obtain comparative threshold cycle (Ct) values of the target genes. GAPDH was used as an internal control. The relative fold-change in gene expression was calculated using the $2^{-\Delta\Delta C_t}$ method.

Western blot analysis

Proteins were obtained from BMDMs, CFs, Raw264.7 cells, the co-culture system, and myocardial tissues. Cells or tissues were homogenised in RIPA buffer containing protease and phosphatase inhibitors. After measuring protein concentration, the proteins were separated by SDS-PAGE and transferred onto a polyvinylidene difluoride membrane (Millipore, Billerica, MA, USA). The membrane was blocked with non-fat dry milk (5%) or bovine serum albumin (5%) and incubated with primary antibodies, followed by secondary antibodies. Finally, the membranes were visualised using an ECL substrate (Thermo Fisher Scientific).

Protein co-immunoprecipitation

Co-immunoprecipitation (Co-IP) was performed using a Co-IP Kit (Absin, Shanghai, China). Briefly, approximately 2×10^6 cells in the co-culture system with or without ITIH5 overexpression were sonicated three times for 20 s each in 500 μ L of ice-cold lysis buffer before being centrifuged at $14\,000 \times g$ for 10 min at 4 °C. Supernatants were collected as whole-cell lysates. Cell lysates were incubated overnight at 4 °C with ITIH5 antibody (2 μ g) or CD44 antibody (2 μ g) and control IgG (1 μ g). Protein A- and protein G-Sepharose (5 μ L) were added to the cell lysates and incubated overnight at 4 °C. After 1 min of centrifugation at $12\,000 \times g$, the beads were collected and washed three times with the wash buffer. The beads were boiled in 40 μ L loading buffer (1 \times) for 5 min and centrifuged for 1 min at $14\,000 \times g$ and 4 °C. The supernatant was collected for subsequent western blotting experiments.

Cell immunofluorescence

For immunofluorescence, cell monolayers were fixed with 4% paraformaldehyde and treated with 0.3% Triton X-100. After three washes with PBS, the cells were blocked with 5% bovine serum albumin for 40 min. The cells were then incubated with primary antibodies, followed by fluorescently-labelled secondary antibodies and

Hoechst staining. The results were observed under a confocal microscope (ZEISS).

CFs EdU staining

EdU staining was performed using the EdU-488 Cell Proliferation Detection Kit (Beyotime). The CFs were incubated with the EdU solution for 12 h in an incubator with 5% CO₂ at 37 °C. Cells were fixed and stained with Alexa Fluor 488. Nuclear counterstaining was performed using Hoechst33342. The final images were observed using a fluorescence microscope (Leica).

Flow cytometry (FCM) analysis

BMDMs or cells in co-culture system were digested with trypsin, washed twice with PBS, and suspended in 100 μ L staining buffer (10^6 cells per tube). Cell suspensions were incubated at 4 °C for 10 min with 1 μ L purified CD16/32 antibody to block non-specific Fc sites (BioLegend, CA, USA). Cells were then labelled with APC anti-mouse F4/80 (BioLegend) and PE-CY7 anti-mouse CD11b (BioLegend) at 4 °C for 20 min protected from light. Then, 150 μ L Fix/Perm buffer (BioLegend) was added and the cells were incubated at room temperature for 20 min protect from light. After washing with 1 \times Perm wash buffer (BioLegend) three times and resuspend with 100 μ L 1 \times Perm wash buffer, cells were labelled with BV421 anti-mouse CD206 (BioLegend) at room temperature for 20 min protected from light. After washing twice with staining buffer, PBMCs were resuspend with in 400 μ L staining buffer. Flow cytometry was performed using a Beckman CytoFLEX instrument (Beckman Coulter Inc., USA). All data were evaluated using FlowJo software.

Apoptosis FCM analysis

FCM analysis of apoptosis was performed using an Annexin V-FITC/PI apoptosis kit (BDBiosciences, CA, USA, cat# 556,547). Briefly, CFs or cells in co-culture system were digested with trypsin and then collected, washed twice with PBS, and suspended with 100 μ L binding buffer (10^6 cells per tube). Then, 5 μ L Annexin V-FITC and PI were added in each tube and incubated with cell suspension at room temperature for 15 min protect from light. 400 μ L of 1 \times Binding Buffer was added in each tube to make the volume of each tube about 500 μ L. Flow cytometry was performed using a Beckman CytoFLEX instrument (Beckman Coulter Inc.). All data were evaluated using FlowJo software.

Statistical analyses

SPSS26.0 and GraphPad Prism were used for statistical analysis and graphical presentation. Normal distribution measurement data were expressed as mean \pm standard deviation. Independent sample t-test was used for

the comparison of normal distribution data between two groups, non-parametric test (Kruskal–Wallis test) was used for data with non-normal distribution. Counting data are expressed as frequency or percentage (n %), and the chi-square test was used for comparison between groups. Single-factor linear regression was used to evaluate the risk factors for peripheral ITIH5 levels, and risk factors with statistical differences in the single-factor regression were included for further multifactor stepwise linear regression. Single-factor logistic regression was used to evaluate the diagnostic value of each risk factor for ICM, and the risk factors with statistical differences in single-factor regression were included in the multifactor stepwise logistic regression, while receiver operating characteristic (ROC) curves were used to calculate the area under the curve (AUC) and evaluate specificity and sensitivity. To include all the risk factors affecting ITIH5 level, $P < 0.1$ was considered statistically significant in the single-factor linear regression model, while $P < 0.05$ was considered statistically significant in other statistical tests.

Results

ITIH5 as a potential marker of ischemic cardiomyopathy

To explore potential molecular targets for the treatment of ICM, three open-access microarray datasets in the GEO database were merged, and batch effect correction and standardisation were performed on the merged datasets (Additional file 1, Figure S1a, b). After converting the probe names into gene symbols, 18,813 genes and 206 DEGs were identified (Fig. 1a). Then, we conducted functional enrichment analysis of GO and KEGG pathways in DEGs, which suggested that DEGs mainly enriched in functional gene clusters including “extracellular matrix organization”, “collagen-containing extracellular matrix”, “extracellular matrix structural constituent” and signaling pathways such as “complement and coagulation cascades”, “Chagas disease”, “viral protein interaction with cytokine and cytokine receptor” (Fig. 1b).

We further identified the genes that were significantly associated with ICM. A total of 2,000 genes with the

highest median deviation were used to construct co-expression modules using the WGCNA algorithm, which could appropriately assess the scale-free topology of the network. When the correlation coefficient threshold was 0.9, the soft-thresholding power was selected to six (Fig. 1c). Through WGCNA analysis, 13 co-expression modules were constructed (Fig. 1d). The module comprising the most genes (464 genes) was turquoise. To identify correlations between gene modules and clinical phenotypes, we conducted module-trait correlations between ICM and NF samples and found that the turquoise module was significantly correlated with ICM (Fig. 1e). Furthermore, all the genes in the turquoise module were significantly associated with ICM (Fig. 1f).

Next, 106 genes were identified by intersecting DEGs and genes in the turquoise module (Fig. 1g), and a random forest model was constructed based on the expression levels of these 106 genes. The model error tended to stabilise when $mtry = 3$ and $ntree = 500$ (Fig. 1h). Based on the MeanDecreaseGini method, 25 key genes with $MeanDecreaseGini > 2$ were selected (Fig. 1i). ITIH5 had the highest Mean Decrease Gini score, representing a significant correlation in the ICM assessment model. Two external datasets were used to verify the differential expression of ITIH5 and evaluate its diagnostic value. The results suggested that ITIH5 expression levels in the myocardial tissues of ICM samples were significantly higher than those in NF samples (Fig. 1j), with satisfactory diagnostic value (Fig. 1k).

ITIH5 as a peripheral blood marker of ICM

ITIH5 can be detected as a secreted protein in human peripheral blood [20]. To further explore the diagnostic value and clinical translational possibility of ITIH5 in patients with ICM, we collected peripheral blood and basic clinical information from 53 patients with ICM and 40 NF controls (detailed baseline information is listed in Additional file 1, Table S3) and detected ITIH5 protein levels in the peripheral blood by ELISA. Subsequently, we divided the patients into several groups according to LVEF (HFpEF, HFmrEF, and HFrEF) and NYHA cardiac

(See figure on next page.)

Fig. 1 ITIH5 as a potential marker of ischemic cardiomyopathy. **a** Volcano map of DEGs. **b** GO and KEGG enrichment analysis of DEGs. **c** Analysis of the scale-free fit index for various soft thresholding powers (Left) and analysis of the mean connectivity for various soft-thresholding powers (Right). **d** Hierarchical cluster analysis was conducted to detect co-expression clusters with corresponding colour assignments. Each colour represents a module in the constructed gene co-expression network by WGCNA. **e** Relationships of consensus module and clinical trait, with different colours representing different modules. Each row corresponds to a module and columns represent their correlations with the traits. **f** Module significance values of those co-expression modules associated with ICM (module significance value indicated the summary of gene significance of all genes in each module, and different colours of column indicated different modules). **g** Intersection genes of DEGs and turquoise module genes. **h** The relationship between the number of random forest decision trees and error rate. **i** Ordering of gene importance by MeanDecreaseGini method. **j** The ITIH5 expression level in the cardiac tissue of each group in the external validation datasets. **k** Diagnostic efficacy assessment (ROC curve) of the ITIH5 gene expression level in the external validation datasets

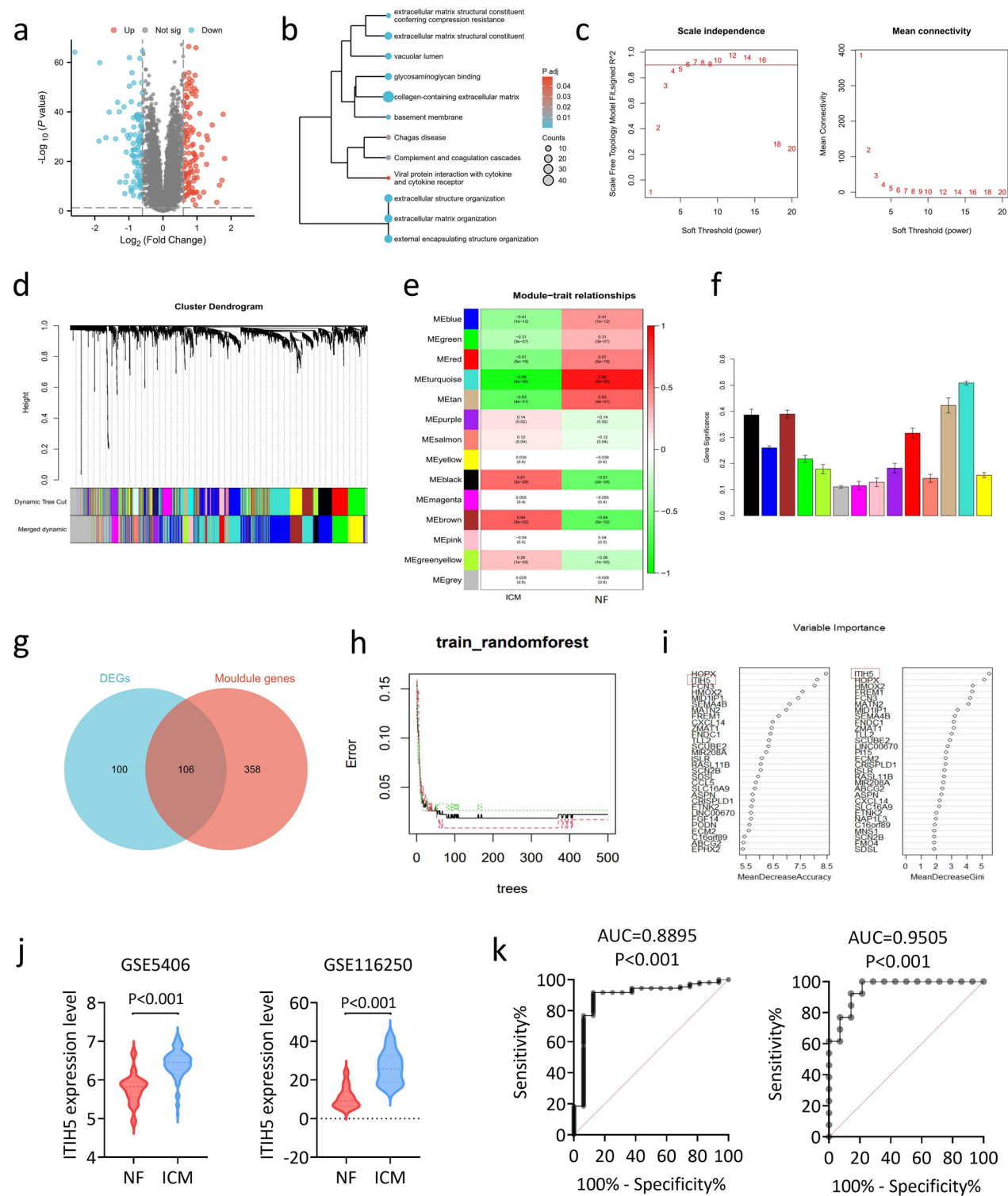


Fig. 1 (See legend on previous page.)

function classification (NYHA II, III, and IV) and analysed the ITIH5 levels in each group. The level of ITIH5 in patients with ICM was significantly higher than that in NF controls (Additional file 1, Figure S2a). Nevertheless,

we did not observe a gradual increase in ITIH5 levels along with a deterioration of cardiac function and a decrease in LVEF (Additional file 1, Figure S2b).

Subsequently, we conducted a linear regression based on ITIH5 level, and found that the ITIH5 level was correlated with multiple factors, including gender ($\beta=5.92$, $P=0.083$), diabetes ($\beta=7.532$, $P=0.04$), body mass index (BMI) ($\beta=0.736$, $P=0.097$), white blood cells (WBC) ($\beta=1.358$, $P=0.04$), albumin ($\beta=-1.454$, $P=0.003$), serum total cholesterol ($\beta=-2.379$, $P=0.087$), c reaction protein (CRP) ($\beta=0.166$, $P=0.016$), LVIDd ($\beta=0.485$, $P=0.009$), LVEF ($\beta=-0.429$, $P=0.000$), pulmonary artery pressure (PAP) ($\beta=5.371$, $P=0.07$) and NYHA classification ($\beta=5.854$, $P=0.000$) (Additional file 1, Table S4). A stepwise linear regression analysis was performed with ITIH5 level as the dependent variable, and gender, diabetes mellitus, BMI, WBC, serum albumin, serum total cholesterol, CRP, LVIDd, LVEF, PAP and NYHA classification as the independent variables. The results demonstrated that peripheral blood ITIH5 levels were associated with BMI ($\beta=0.919$, $P=0.023$), CRP ($\beta=0.144$, $P=0.024$), and LVEF ($\beta=-0.409$, $P=0.000$) (Additional file 1, Table S5).

To clarify the diagnostic value of ITIH5 levels in ICM, risk factors and peripheral blood ITIH5 levels were included in univariate logistic regression analysis. The results suggested that sex, age, diabetes, atrial fibrillation, WBC count, albumin, glomerular filtration rate (GFR), low density lipoprotein (LDL), CRP, and ITIH5 were all risk factors for ICM (Additional file 1, Table S6). The association between ITIH5 and ICM was further examined using a multivariate logistic model adjusted for sex, age, diabetes, atrial fibrillation, WBC count, albumin level, GFR, LDL level, CRP level, and ITIH5 level. We found that ITIH5 elevation was independently associated with the risk of ICM (OR=1.132; 95% CI 1.057–1.213) (Additional file 1, Table S7). Sex, atrial fibrillation, and GFR were independently associated with ICM risk. We further evaluated the ability of ITIH5 to diagnose ICM using ROC curves. The AUC of ITIH5 levels was 0.806 (95% CI 0.716–0.896), and the predictive ability was better or no worse than that of sex (AUC=0.712; 95% CI 0.72–0.822), GFR (AUC=0.811; 95% CI 0.723–0.899) and atrial fibrillation (AUC=0.626; 95% CI 0.513–0.738) (Additional file 1, Figure S2c). The cut-off value of the ITIH5 level was 26.488 ng/mL, with a sensitivity of 83% and specificity of 67.5%, suggesting that it may be a potential ICM biomarker.

ITIH5 expression was up-regulated after MI, expressed by fibroblasts, and localized to ECM

We used a mouse model of MI to further explore the biological functions of ITIH5 under ischaemic conditions. First, the dynamic alterations in the expression of ITIH5 were clarified. The results suggested that ITIH5 protein (Fig. 2a) and mRNA (Fig. 2b) expression was upregulated

in the acute phase (within 3 d) after MI, reached a peak 7–14 d after MI, and remained high. Further, immunofluorescence detection was performed in mouse heart tissue 7 d after MI, and the results indicated that ITIH5 fluorescence intensity in the infarcted areas was significantly increased, which coincided with the infarction areas shown by H&E and Sirius Red staining (Fig. 2c). To clarify the differences in ITIH5 expression between cell populations and their subcellular localisation, we first analysed the mouse scRNA-seq dataset. The results suggested that ITIH5 was mainly expressed by fibroblasts in both normal and infarcted myocardium (Fig. 2d). ITIH5 mRNA expression levels between CFs, cardiomyocytes and immune cells were further detected and verified the ITIH5 expression was significantly higher in CFs (Additional file 1, Figure S3a). Tissue immunofluorescence co-localization was further used to show that ITIH5 was co-located with collagen I rather than vimentin, confirming that ITIH5 was expressed by fibroblasts but eventually secreted into the ECM (Fig. 2e). Consistent with the phenomenon observed by Martin et al. [19], ITIH5 protein levels were significantly reduced after fibroblasts were treated with low trypsin concentrations prior to lysis. We also detected a small amount of ITIH5 protein in the supernatant of the cell culture medium, which was significantly reduced compared to that in the original cell lysate (Fig. 2f). In vitro immunofluorescence co-localization demonstrated that ITIH5 mainly distributed around the cell border (Additional file 1, Figure S3b). These in vitro results suggested that most of the ITIH5 detected in the whole-cell lysate was extracellular and attached to the cell surface, rather than being distributed freely in the culture supernatant.

ITIH5 exacerbates fibrotic remodelling after MI

To further elucidate the biological function of ITIH5, AAV9-pPOSTN-shITIH5 was used to inhibit ITIH5 expression in the CFs. Based on temporal changes in ITIH5 protein expression, two different time points were selected to observe the effects of ITIH5 downregulation on the risk of death, cardiac function, tissue morphology, and biological function of mice after MI: 7 d (reparative phase) and 28 d (mature phase). First, AAV treatment significantly knocked down ITIH5 expression in infarcted cardiac tissues (Additional file 1, Figure S4). Although ITIH5 downregulation did not significantly alter the mortality rate within 28 d after MI in mice, it did significantly increased mortality within 7 d after MI in mice (Fig. 3a). Echocardiography results suggested that ITIH5 downregulation improved long-term (28 d) cardiac function in mice after MI to a certain extent, which manifested as reduced LVIDd and mild remission of LVEF and LVFS (Fig. 3b). In line with this, ITIH5

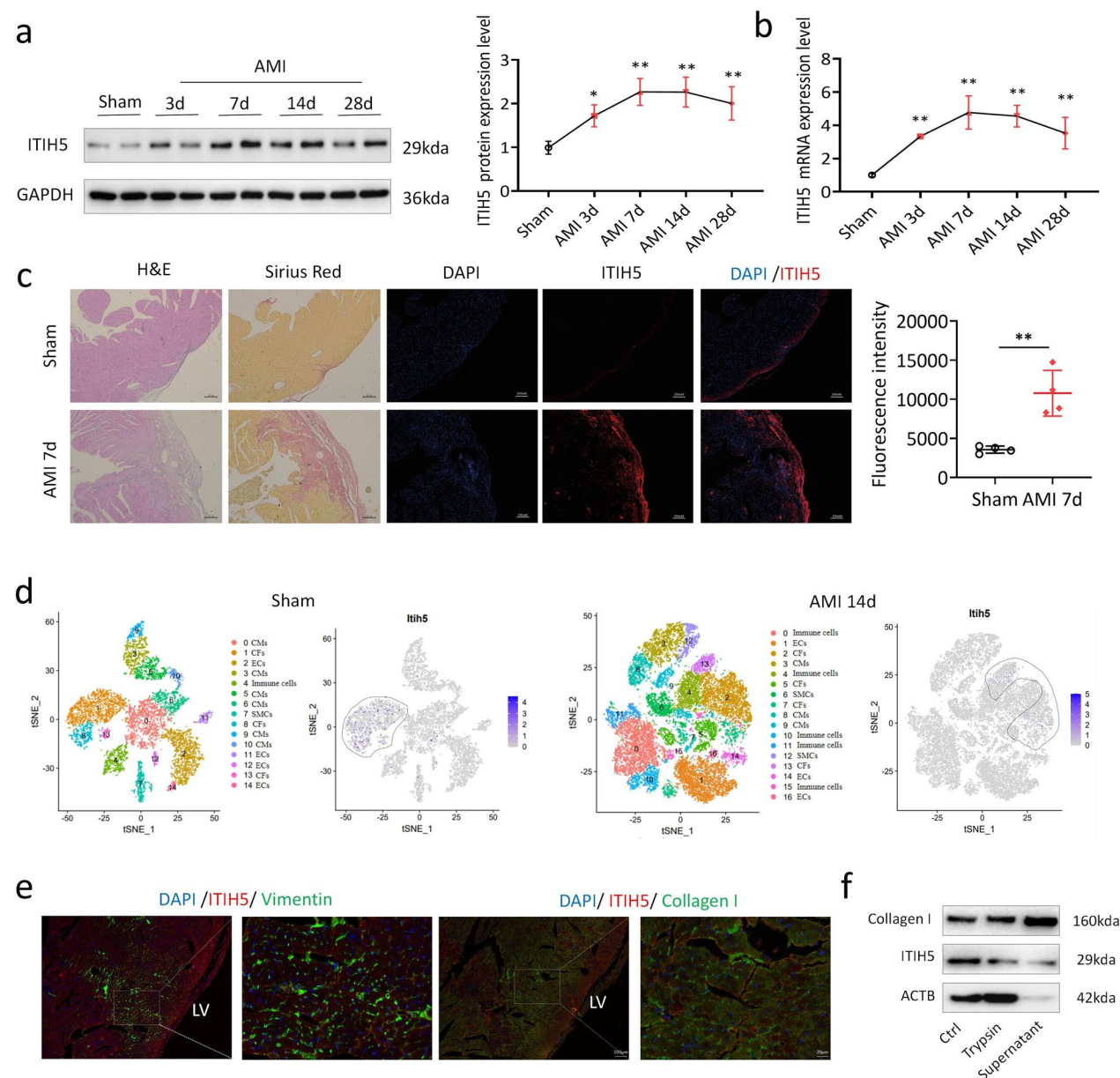


Fig. 2 ITIH5 expression was up-regulated after MI, expressed by fibroblasts, and localized to ECM. **a** The temporal changes of ITIH5 protein expression in the cardiac tissue after MI (left: western blot, right: statistical graph) ($n = 4$). **b** The temporal changes of ITIH5 mRNA expression levels in cardiac tissue after MI ($n = 4$). **c** Representative immunofluorescence images of ITIH5 in the infarction areas 7 d after MI and the H&E and Sirius Red staining images of the corresponding tissue samples. **d** tSNE map and ITIH5 expression level distribution of cardiac tissue of Sham and MI model mice. **e** Immunofluorescence co-localization of ITIH5 and vimentin or ITIH5 and collagen I in cardiac tissue. **f** Representative western blot of ITIH5 and collagen I protein expression levels in normal fibroblasts and trypsin-treated fibroblast culture medium supernatants. Data presented as mean \pm SD. *, $P < 0.05$; **, $P < 0.01$

downregulation significantly reduced serum NT-proBNP levels in the mature phase (28 d) after MI (Fig. 3c). Although H&E staining indicated that ITIH5 downregulation did not ameliorate the infarcted area or ventricular wall thickness in mice after MI (Fig. 3d), Masson's trichrome staining indicated that ITIH5 downregulation

significantly inhibited the degree of cardiac fibrosis in mice at all phases after MI (Fig. 3e).

Further studies are needed to evaluate the role of ITIH5 in fibrotic remodelling after MI. First, we evaluated the apoptosis and proliferation of CFs in the mature phase after MI. The results indicated that there were more

TUNEL-positive and less Ki67-positive CFs in the infarct area of the ITIH5 KD mice (Fig. 3f). These results suggest that ITIH5 downregulation inhibits CFs proliferation and promotes CFs apoptosis. In addition, downregulation of ITIH5 expression had no significant effect on post MI angiogenesis (Fig. 3f). In addition, western blotting was used to detect CFs activation status in the infarction area at the reparative phase after MI, as fibroblasts began to activate and remain active 3–7 d after MI [5]. These results suggest that collagen synthesis and myofibroblast transdifferentiation in ITIH5 KD mice were significantly weakened (Fig. 3g). Overall, we observed that ITIH5 downregulation significantly improved cardiac function after MI but had no significant effect on infarct size. Furthermore, ITIH5 downregulation primarily inhibited fibrotic activation during the repair phase, increased fibroblast apoptosis, and inhibited proliferation during the maturation phase after MI.

ITIH5 promotes CF proliferation, migration, and cell survival rather than activation

In vivo experiments suggested that ITIH5 has a wide range of regulatory effects on the entire stage of fibrosis after MI. We validated the direct regulatory function of ITIH5 in CFs in vitro. First, CFs were treated with Ang II or hypoxia for 24 h, respectively, and the mRNA and protein expression levels of ITIH5 were detected. These results suggested that both Ang II and hypoxia induced the upregulation of ITIH5 mRNA (Fig. 4a) and protein expression (Fig. 4b). Similar conclusions were obtained by immunofluorescence detection (Additional file 1, Figure S5a). To further clarify the function of ITIH5 in CFs, we used siRNA to inhibit ITIH5 gene expression or lentivirus to overexpress ITIH5. Both siRNA and lentivirus stably inhibited or increased ITIH5 expression in fibroblasts (Fig. 4c and Additional file 1, Figure S5b). Subsequently, we examined whether ITIH5 downregulation or overexpression affected CFs activation. Western blot analysis indicated that both ITIH5 downregulation and overexpression altered only the expression of collagen III (Fig. 4c and Additional file 1, Figure S5b). Collagen I, the most important component of ECM and α -SMA, a marker of myofibroblasts, showed no significant changes

under altered ITIH5 expression levels (Fig. 4c and Additional file 1, Figure S5b). ITIH5 has limited ability to directly regulate fibroblast activation, collagen synthesis, and myofibroblast transformation.

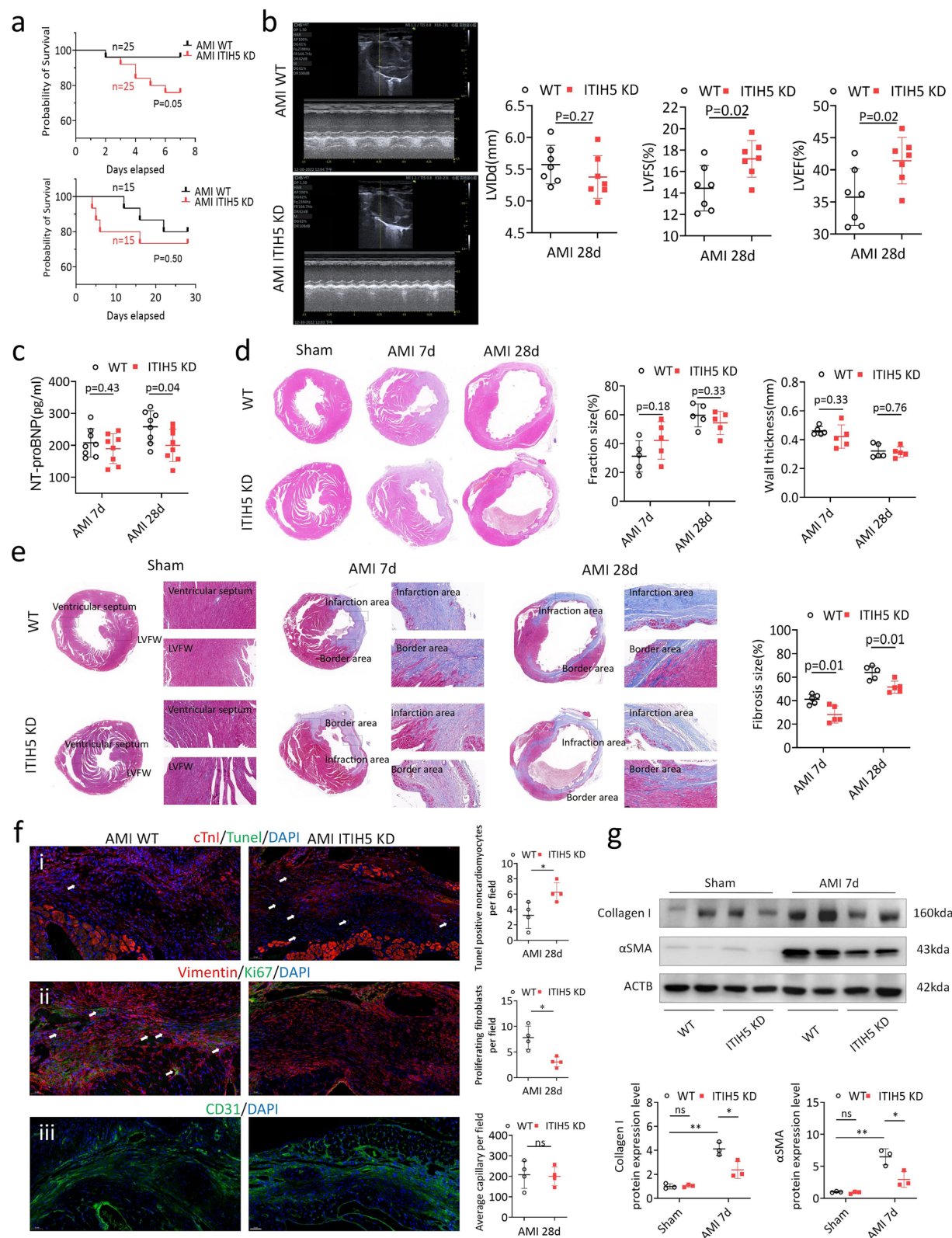
As ITIH5 is considered a potential matricellular protein, it may play a regulatory role in cell proliferation, migration, and cell survival [10, 11] which was identified in our mouse experiments; however, this has not been described in detail in previous studies. Further studies are required to verify the matricellular function of ITIH5 in vitro. As hypothesised, the results suggested that ITIH5 overexpression promoted the regeneration of a large number of undifferentiated fibroblasts (Additional file 1, Figure S6a). Subsequently, qRT-PCR confirmed that ITIH5 overexpression promoted the expression of collagen III and proliferation markers, such as Ki67 and PCNA (Additional file 1, Figure S6b). Similarly, results using the CCK8 assay showed that ITIH5 downregulation reduced the number of fibroblasts (Fig. 4d), and EdU staining confirmed that ITIH5 downregulation significantly inhibited the proliferation of CFs (Fig. 4e). In contrast, ITIH5 protected the survival of CFs under serum-free conditions, as manifested by ITIH5 downregulation increased cleaved caspase 3 and Bax protein expression levels (Fig. 4f), and increased the proportion of apoptotic cells (Fig. 4g). Finally, we examined whether ITIH5 could regulate CFs migration. The results suggested that ITIH5 downregulation significantly inhibited Ang II-induced CF migration (Fig. 4h).

ITIH5 regulates macrophage function during the reparative phase after MI

In vitro experiments revealed a limited regulatory function of ITIH5 in CFs activation which was inconsistent with the significant fibrotic response observed in vivo, suggesting that ITIH5 may indirectly regulate post MI fibrosis through other pathways. We thus conduct mRNA sequencing on the mice infarction myocardium of each group at 7 days after MI. A total of 380 DEGs were confirmed (Fig. 5a). GO enrichment demonstrated that DEGs were enriched in 'positive regulation of ERK1 and ERK2 cascade', 'myeloid leukocyte migration', 'chemokine-mediated signaling pathway', 'granulocyte migration', 'cytokine

(See figure on next page.)

Fig. 3 ITIH5 exacerbates fibrotic remodelling after MI. **a** Survival curves of mice in the WT and ITIH5 knockdown groups within 7 and 28 d after MI. **b** Representative echocardiography images of mouse heart and statistics analysis of LVEF, LVFS and LVIDd in the WT and ITIH5 knockdown groups 28 d after MI. **c** The statistical analysis of NT-proBNP in the WT and ITIH5 knockdown groups 7 and 28 d after MI. **d** Representative H&E staining images and statistical analysis of infarction area size and ventricular wall thickness in the WT and ITIH5 knockdown mice 7 and 28 d after MI. **e** Representative Masson's trichrome staining images and statistical analysis of fibrosis area size in the WT and ITIH5 knockdown mice at 7 and 28 d after MI. **f** Immunofluorescence or immunofluorescence co-localization of (i) cTnI and TUNEL, (ii) vimentin and Ki67, and (iii) CD31 in WT and ITIH5 knockdown groups 7 d after MI. **g** Representative western blots and statistical analysis of collagen I and α -SMA protein expression levels in the WT and ITIH5 knockdown groups 7 d after MI. Data presented as mean \pm SD. *, $P < 0.05$; **, $P < 0.01$; ***, $P < 0.001$



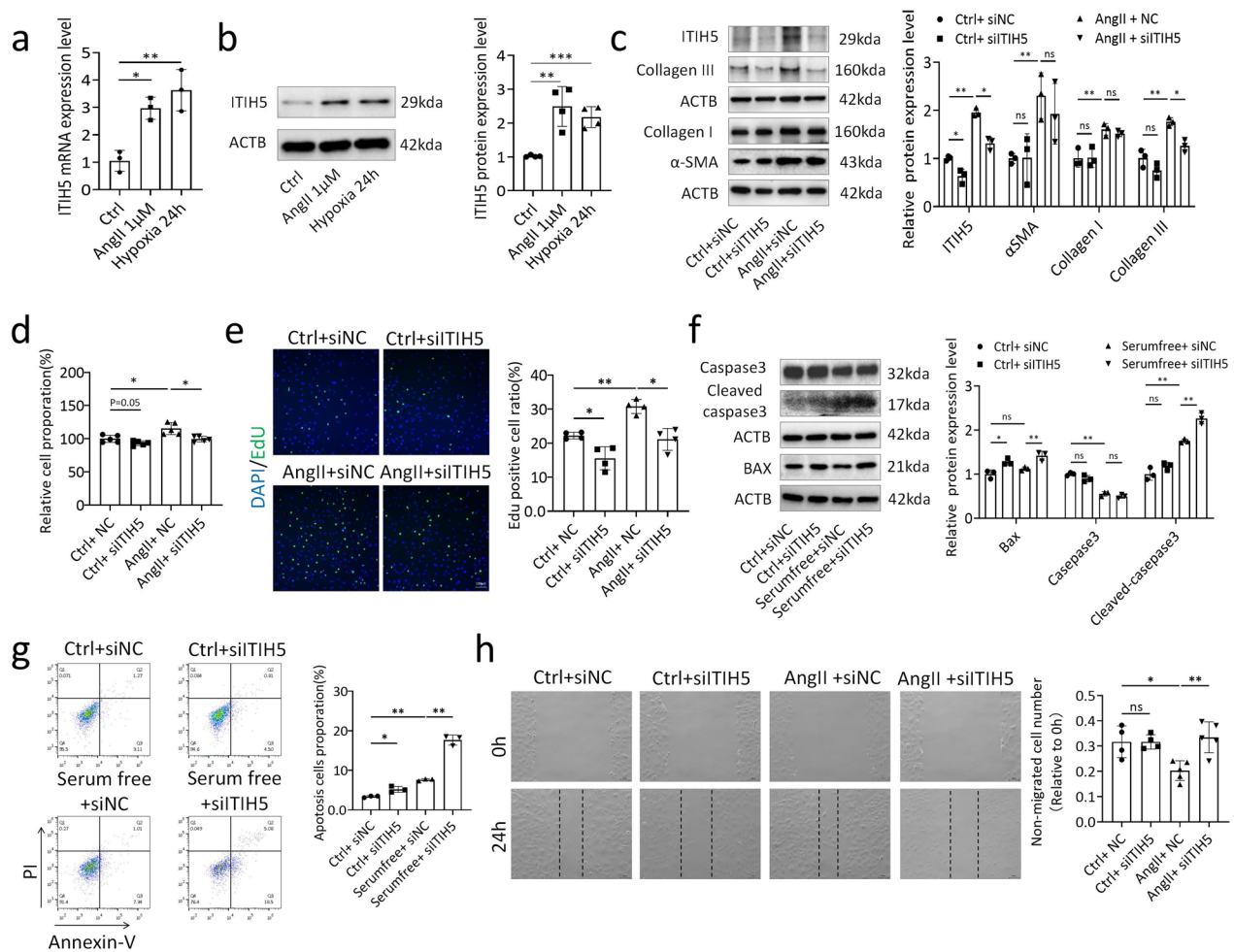


Fig. 4 ITIH5 promotes CFs proliferation, migration, and cell survival rather than activation. **a** ITIH5 mRNA expression levels in CFs under Ang II and hypoxia treatment. **b** Representative western blot and statistical analysis of ITIH5 protein expression levels in CFs under Ang II and hypoxia treatment. **c** Representative western blots and statistical analysis of collagen III, collagen I, α-SMA and ITIH5 protein expression levels in CFs under different treatments. **d** Cell counting of CFs under different treatments. **e** Representative images of EdU staining and statistical analysis of CFs under different treatments. **f** Representative western blots and statistical analysis of Bax, caspase 3, and cleaved-caspase 3 protein expression levels in CFs under different treatments. **g** Representative flow cytometry images and statistical analysis of CFs apoptosis under different treatments. **h** Representative images and statistical analysis of CFs migration under different treatments. Data presented as mean ± SD. *, $P < 0.05$; **, $P < 0.01$; ***, $P < 0.001$; ns, not significant

activity', 'chemokine activity', 'Cytokine-cytokine receptor interaction', and 'Chemokine signaling pathway', indicating enhanced immune cell chemotaxis, and Extracellular signaling transportation (Fig. 5b). Furthermore, GSEA analysis highlighted the inhibition of 'Acute inflammatory response', and 'Cytokine cytokine receptor interaction' caused by ITIH5 downregulation (Fig. 5c). Previous studies have suggested that ITIH5 has a wide range of immune regulatory functions [20, 22]. However, no study has reported its immunological regulation in the process of tissue repair after MI. Seven days after MI, at the most active stage of immune-mediated fibrosis repair, we detected major immune population

changes between ITIH5 KD and WT mice. The results indicated that ITIH5 downregulation significantly inhibited macrophage infiltration in the infarction area compared to that of neutrophils and lymphocytes (Fig. 5d). Macrophages are the most important immune cell population in the myocardial tissue 7 d after MI, and ITIH5 protein levels reach their peak expression at that time [24]. Therefore, we performed qRT-PCR to detect macrophage-related genes and explore the functional changes in macrophages regulated by ITIH5. The results suggested that down-regulation of ITIH5 widely inhibited macrophages differentiation and maturation (CD68, ADGRE1, CSF1R, ITGAM), phenotype transformation

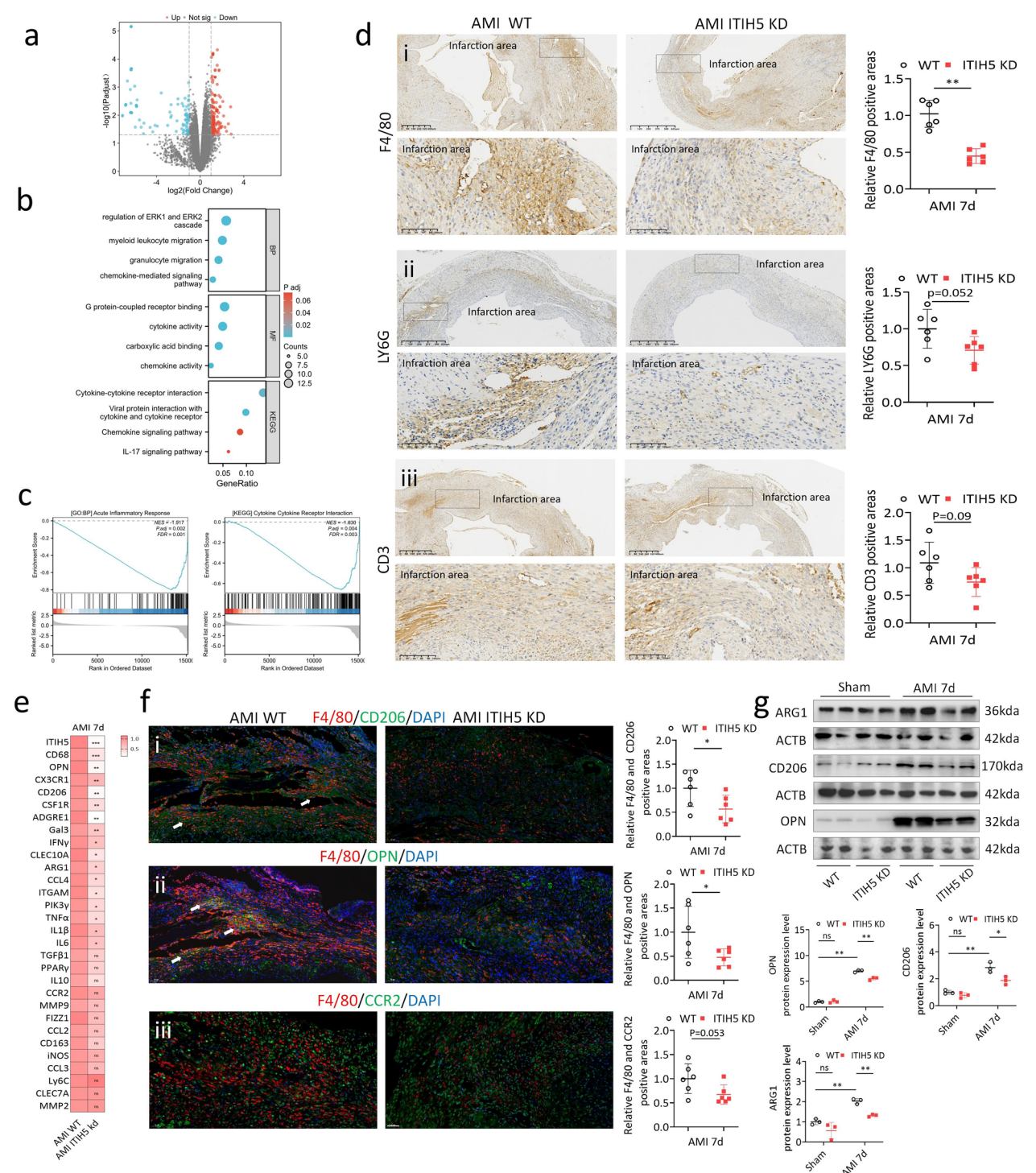


Fig. 5 ITIH5 regulates macrophage function during the reparative phase after MI. **a** Volcano plot of DEGs. **b** GO and KEGG enrichment analyses of DEGs. **c** GSEA enrichment analyses of DEGs. **d** immunohistochemical staining of (i) F4/80, (ii) LY6G and (iii) CD3 in the WT and ITIH5 knockdown groups 7 d after MI. **e** mRNA expression levels of macrophage-related genes in the WT and ITIH5 knockdown groups 7 d after MI. **f** Immunofluorescence co-localization of (i) F4/80 and CD206, (ii) F4/80 and OPN, (iii) F4/80 and CCR2 in the WT and ITIH5 knockdown groups 7 d after MI. **g** Representative western blots and statistical analysis of ARG1, CD206, and OPN protein expression levels in the WT and ITIH5 knockdown groups 7 d after MI. Data presented as mean \pm SD. *, $P < 0.05$; **, $P < 0.01$; ***, $P < 0.001$; ns, not significant

(MRC1, ARG1, IFN γ , CLEC10A) and other cytokines and secreted proteins expression levels (SPP1, Gal3, CCL4, TNF α , IL1 β , IL6) (Fig. 5e).

Immunofluorescence co-localization was used to verify the most differentially expressed genes. The results showed that ITIH5 downregulation significantly inhibited the proportion of CD206 and OPN-positive macrophages in the infarcted area (Fig. 5f). A slight reduction in CCR2⁺ macrophages in the ITIH5 KD mouse infarction area (Fig. 5f). Western blotting also verified that CD206, OPN, and ARG1 protein levels were downregulated in the infarcted areas of the ITIH5 KD mice (Fig. 5g). Overall, ITIH5 mediated extensive macrophage responses after MI.

ITIH5 promotes macrophages pro-fibrotic phenotype transition by mediating fibroblast/macrophage crosstalk

In vivo experiments suggested that the ITIH5-regulated severe fibrotic response may be mediated by macrophage phenotype transformation. Therefore, we investigated the effect of ITIH5 on macrophage function by knocking down or overexpressing ITIH5 in macrophages. Western blotting and qRT-PCR were used to confirm the expression levels of significant DEGs detected in vivo. The results indicated that CD206, OPN, ARG1, and CD68 could be representative genes which were significantly up-regulated in Raw264.7 cells overexpressing ITIH5 and downregulated in siRNA-treated BMDMs both at the mRNA and protein levels (Additional file 1, Figure S7 and S8a, b). Further verification by FCM confirmed that ITIH5 KD inhibited the expression of the macrophage membrane receptor CD206 (Additional file 1, Figure S8c).

We previously found that CFs are the main cell types expressing ITIH5. Considering that ITIH5 is mainly distributed in the ECM and may be attached to the cell membrane and rarely distributed in the culture medium supernatant (Fig. 2f, Figure S3b), the Transwell-based co-culture model was not applicable in this study, such that a direct cell-to-cell interaction co-culture model was used to explore the effects of CFs-derived ITIH5 derived on macrophages. We constructed a co-culture model of direct cell–cell interactions (Fig. 6a). Surprisingly, CFs had a higher ITIH5 expression level than macrophages, which further increased in the fibroblast/macrophage co-culture system (Fig. 6b). Measurement of mRNA and protein levels of macrophage and CFs markers in the ITIH5-overexpressed fibroblast/macrophage co-culture model showed that ITIH5 derived from CFs enhanced macrophage maturation and promoted fibrotic phenotype transformation in the co-culture system (Fig. 6c, d). At the same time, collagen synthesis and myofibroblast

differentiation potential were elevated in the co-culture system when ITIH5 was overexpressed (Fig. 6c, d).

The spatial structure has a crucial impact on the function of macrophages and fibroblasts [26]. Based on the 2D co-culture, this study also used a 3D co-culture model, which can further simulate the regulation of infiltration and interaction between macrophages and CFs (Fig. 6a). Based on previous studies, we selected a 3–4:1 fibroblast/macrophage ratio to construct a 3D spherical co-culture system [27, 28], which aggregated into clusters in the middle of the spheroid and was surrounded by macrophages after 5–6 d, following addition of BMDMs (Additional file 1, Figure S9a). H&E staining of the co-cultured spheroids revealed two different cell types (Additional file 1, Figure S9a). However, appropriate cell numbers and spheroid diameters can provide macrophages with sufficient space for infiltration and avoid cell death in the central spheroid due to hypoxia and nutrient deficiency. Therefore, different cell numbers were used to determine whether cell death occurred in the central spheroids. A total of 4000 cells/well was determined as the initial cell number, as there was no significant difference within 5000 cells (Additional file 1, Figure S9b), the diameter of the spheroid was about 200 μ m. H&E staining also revealed no significant necrotic cell cores in the spheroids (Additional file 1, Figure S9a). Later, the co-cultured cell spheroid was subjected to immunofluorescent staining for CD68, CD206, ARG1, OPN and α SMA, which indicated that CD68-positive monocytes/macrophages were more widely distributed in the centre and surrounding the cell spheroid, and the proportion of CD206- and ARG1-positive cells and the fluorescence intensity of OPN increased in the ITIH5 overexpression group (Fig. 6e). The proportion of α SMA-positive fibroblasts and fluorescence intensity also increased in the ITIH5 overexpression group (Fig. 6e).

ITIH5 mediates fibroblast/macrophage crosstalk via HA and CD44/STAT3 signal

Few studies have confirmed that ITIH5 stabilises the function of ECM HA in inflammatory environments; [19, 21] however, it remains unclear whether ITIH5 can mediate similar biological functions after MI. To determine whether ITIH5-mediated fibrotic remodelling after MI is dependent on HA, HABP was first used to detect the structural characteristics of HA in the infarction area, which suggested that ITIH5 downregulation further promoted the disorder of HA arrangement in this region (Fig. 7a). Further in vitro experiments using the HA synthase inhibitor 4-MU showed that 4-MU could reverse the pro-fibrotic phenotype of macrophages and CFs activation caused by ITIH5 overexpression in the co-culture system (Fig. 7b). HA is widely distributed in the ECM and

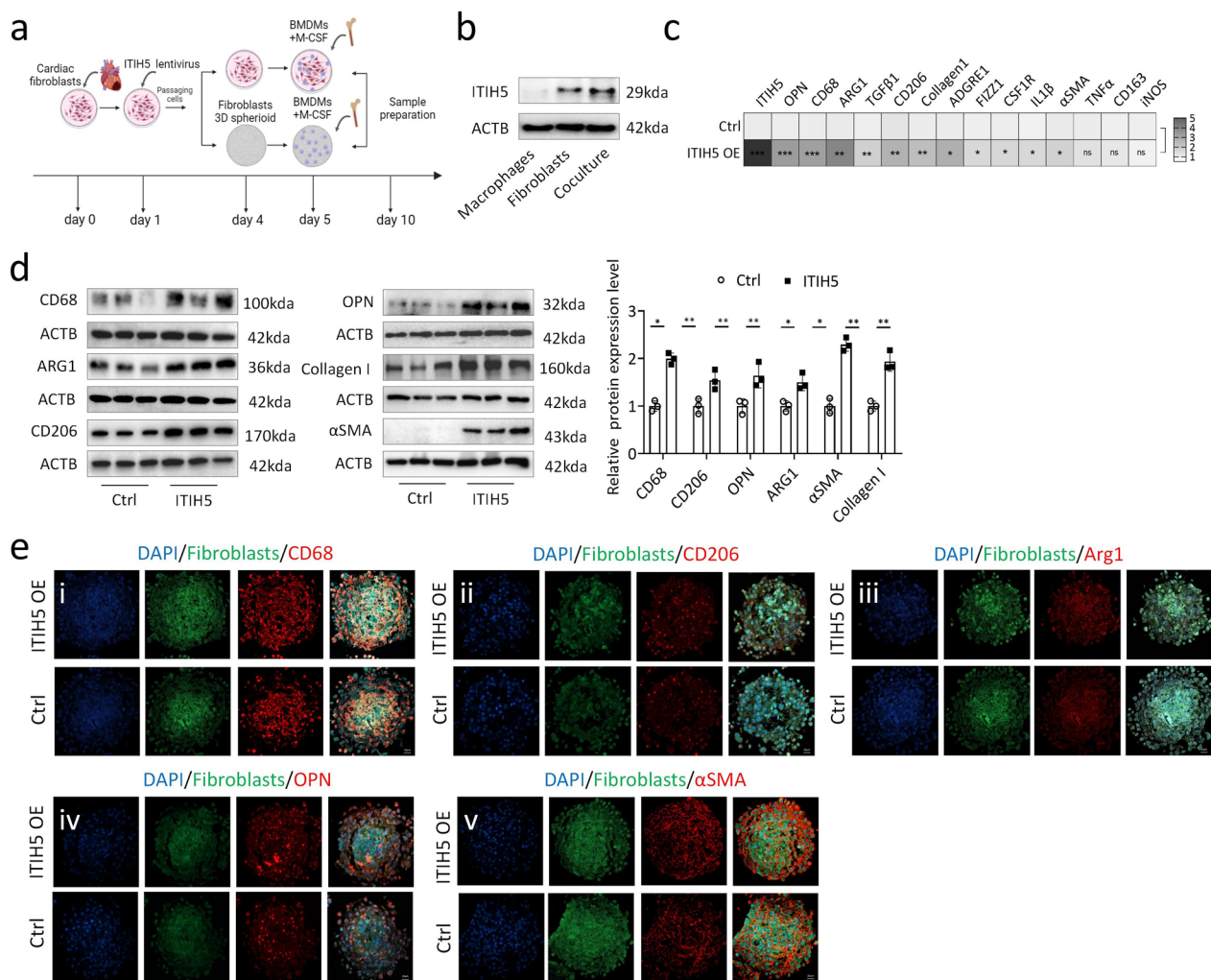


Fig. 6 ITIH5 promotes macrophages pro-fibrotic phenotype transition by mediating fibroblast/macrophage crosstalk. **a** Schematic illustration of the 2D and 3D co-culture system setup. **b** Representative western blot of ITIH5 protein in macrophages, fibroblasts, and the co-culture system. **c** mRNA levels of ITIH5 and other macrophage-related genes in the ITIH5 overexpression and control co-culture systems. **d** Representative western blots and statistical analysis of CD68, OPN, CD206, ARG1, Collagen I, and αSMA protein expression in the ITIH5 overexpression and control co-culture systems. **e** Representative immunofluorescence images of CD68, OPN, ARG1, and αSMA protein expression levels in the ITIH5 overexpression and control 3D co-culture systems. Data presented as mean ± SD. *, $P < 0.05$; **, $P < 0.01$

(See figure on next page.)

Fig. 7 ITIH5 mediates fibroblast/macrophage crosstalk via HA synthesis and CD44. **a** Immunofluorescence of HA of mice cardiac tissue in the WT and ITIH5 knockdown groups at baseline or 7 d after MI. **b** Representative western blots and statistical analysis of CD68, OPN, ARG1, CD206, collagen I, and αSMA protein expression levels in ITIH5 overexpression and control co-culture systems treated with different concentrations of 4-MU. **c** The interaction between ITIH5 and CD44 in different groups was determined by Co-IP. **d** Immunofluorescence images showing co-localization of ITIH5 and CD44 in the ITIH5 overexpression and control co-culture systems (arrows point to macrophages in co-culture system). **e** Representative western blots and statistical analysis of CD68, OPN, ARG1, CD206, collagen I, and αSMA protein expression levels in the ITIH5 overexpression and control co-culture systems treated with CD44-neutralizing antibody and isotype control antibody. **f** Representative western blots and statistical analysis of STAT3 and phospho-STAT3 proteins level in WT and ITIH5 knockdown mice 7 d after MI. **g** Representative western blots of STAT3 and phospho-STAT3 protein expression levels in different groups showing the interaction between CD44 and total/phospho-STAT3 in different groups determined by Co-IP. **h** Immunofluorescence images of phospho-STAT3 of mice cardiac tissue in WT and ITIH5 knockdown groups 7 d after MI. **i** Representative western blots and statistical analysis of CD68, OPN, ARG1, CD206, collagen I, and αSMA protein expression levels in different groups. Data presented as mean ± SD. *, $P < 0.05$; **, $P < 0.01$; ***, $P < 0.001$; #, $P < 0.05$ (compared to the ITIH5 OE group), ## represents $P < 0.001$ (compared to the ITIH5 OE group); ns, no significant difference; OE, overexpression; PCC, Pearson correlation coefficient

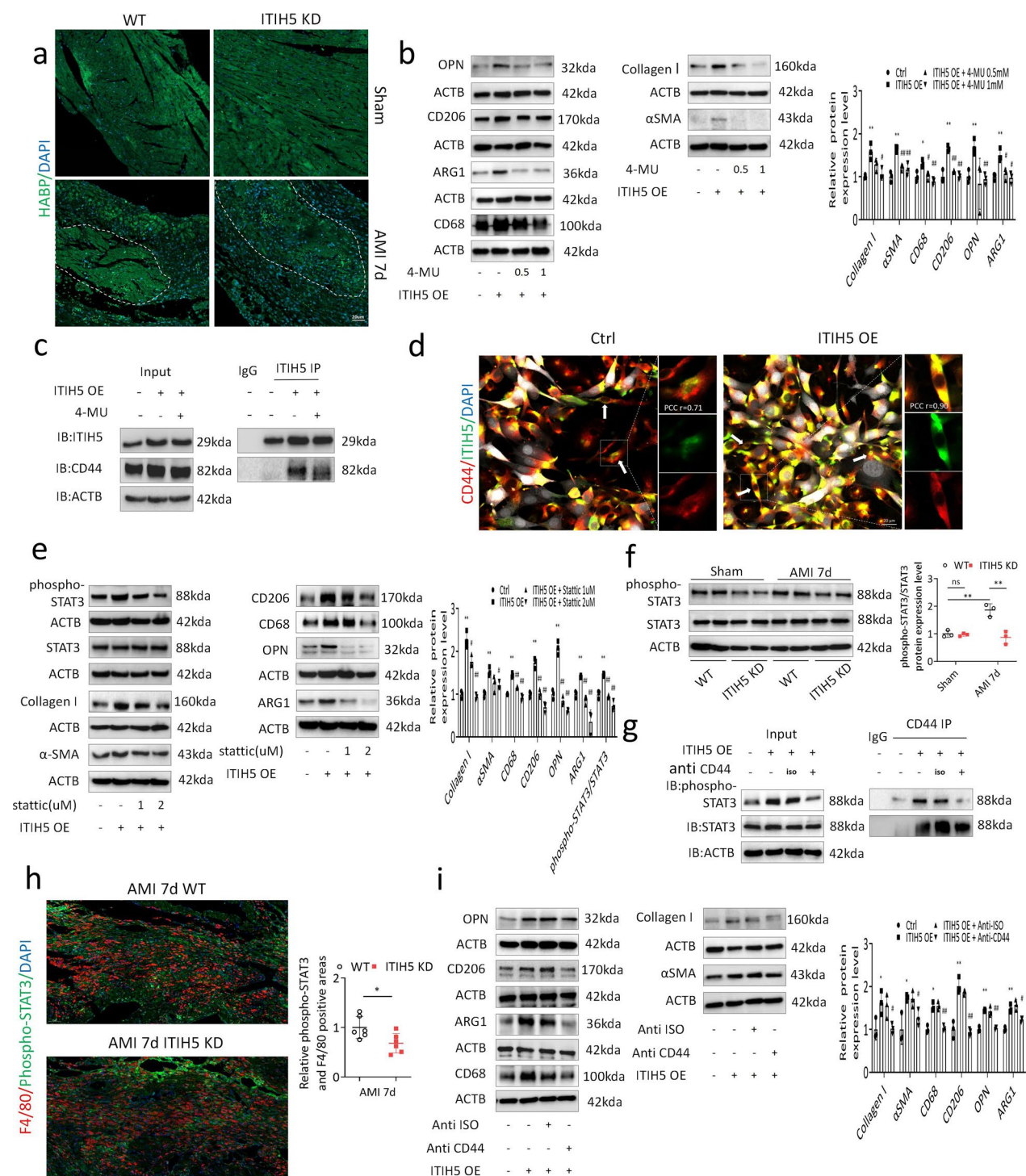


Fig. 7 (See legend on previous page.)

binds specifically to CD44. CD44 is distributed in various cell membranes, such as those of macrophages and fibroblasts, and HA promotes macrophage/myofibroblast-mediated fibrosis by binding to CD44 on macrophages

[29, 30]. To clarify how ITIH5 transduces extracellular signals into macrophages, it is necessary to further examine the relationship between ITIH5 and CD44. First, cell lysates from ITIH5 overexpression and control co-culture

systems were subjected to immunoprecipitation with an ITIH5 antibody, and the expression levels of ITIH5 and CD44 were detected in the lysates and immunoprecipitates, respectively. The results indicated that the ITIH5 protein expression level was significantly increased in the ITIH5 overexpression co-culture system, whereas CD44 expression level was not significantly changed. However, upregulation of ITIH5 significantly promoted its binding to CD44, and inhibition of HA synthesis weakened ITIH5 and CD44 binding ability (Fig. 7c). Similarly, immunofluorescence was used to label ITIH5 protein and the CD44, which suggested that ITIH5 and CD44 were co-localised around the cell membrane, and the degree of co-localisation increased with the upregulation of ITIH5 expression (Fig. 7d), and similar phenomenon was observed in the myocardial infarction area (Additional file 1, Figure S10). Finally, we used CD44-neutralizing antibodies to treat the ITIH5 overexpressed co-culture system. The results showed that blocking CD44 signalling inhibited ITIH5-mediated macrophage differentiation, profibrotic phenotype transformation, and CFs activation (Fig. 7e).

These experiments confirm that ITIH5 affects macrophage function by affecting HA and CD44 signal transduction. Therefore, it is necessary to elucidate the specific downstream signalling pathways of CD44 in macrophages affected by ITIH5. Previous studies have reported that the STAT3 signalling pathway, a key signalling pathway downstream of CD44, is activated during the inflammatory state [31]. Therefore, we first measured the levels of phospho-STAT3 in mouse tissues after MI. Western blotting and tissue immunofluorescence indicated that the level of phospho-STAT3 in macrophages in the myocardial tissue was significantly decreased in ITIH5 KD mice (Fig. 7f, h). To further clarify whether there is a direct interaction between the CD44 and STAT3 pathways, we used a CD44 neutralisation antibody to inhibit CD44 activation and then detected the interaction between CD44 and STAT3 protein and the activation state of the STAT3 signalling pathway in the co-culture system. These results suggest that blocking CD44 can reverse STAT3 phosphorylation level caused by ITIH5 overexpression, which is regulated by its direct interaction with CD44. Thus, blocking CD44 inhibits the ability of ITIH5 to activate STAT3 protein, demonstrated by a reduction in phospho-STAT3 level (Fig. 7g). However, ITIH5 did not directly bind to STAT3 protein (Figure S11a), confirming that ITIH5-mediated phosphorylation of STAT3 is dependent on CD44. Finally, the STAT3 inhibitor Stattic was used to treat the co-culture system, and the results confirmed that the inhibition of STAT3 activation could inhibit ITIH5-mediated macrophage differentiation, profibrotic phenotype transformation, and CFs activation (Fig. 7i, Figure S11b).

Discussion

ITIH5 is a novel ECM protein which is significantly elevated in the myocardium under ischaemic conditions. We conducted studies in patients, animals, and cultured cells to address the impact of ITIH5 on the pathogenesis of cardiac fibrotic remodelling and fibroblast-macrophage crosstalk after MI. Specifically, ITIH5 can be used as a molecular marker in the myocardium and peripheral blood of patients with ICM with satisfactory diagnostic value. In addition, ITIH5 expression was upregulated in the infarcted area after MI and localised to the ECM, promoting macrophage profibrotic phenotype transformation, and eventually exacerbating fibrotic remodelling after MI. Mechanistically, ITIH5 can bind to CD44 on macrophages, which mainly depends on the presence of HA, thereby activating macrophage STAT3 signalling and promoting profibrotic phenotype transformation (Fig. 8).

Determination of ITIH5 levels in the peripheral blood of patients with ICM provides a possibility for clinical translation. In this study, ITIH5 was proven to be an independent risk factor for ICM, although ITIH5 levels can also be affected by risk factors other than cardiac function, such as BMI and CRP. Previous studies have indicated that the adipose tissue is one of the organs with the highest ITIH5 expression levels, and that its expression increases in people with obesity and is highly positively correlated with BMI [16, 22]. In addition, ITIH5 can further regulate the process of lipid differentiation; however, its specific regulatory functions and mechanisms remain controversial [16, 22]. The CRP levels in the peripheral blood are closely related to ITIH5. In addition, ITIH5 regulates inflammatory reactions, including inhibition of pro-inflammatory factors such as TNF- α , IL6, and MCP1 [16, 22], and improves the excessive inflammatory response of inflammatory skin diseases [20]. Interestingly, the ITIH5 levels did not show a tendency toward further elevation with the deterioration of cardiac function and decrease in LVEF, indicating that the ITIH5 level in the peripheral blood can be used as an evaluation index for early heart failure, but cannot determine the severity. Compared to HFrEF, HFpEF is more susceptible to systemic inflammation and secondary cardiac fibrosis [32]. The elevation of ITIH5 may represent a hallmark of abnormal immune response and fibrosis activation. However, extremely abnormal body weight can conceal the upregulation of ITIH5 levels associated with moderate and severe cardiac dysfunction to a certain extent, because moderate and severe cardiac dysfunction is often accompanied by decreased appetite, nutritional disorders, and even dyscrasia. This also suggests that the interference caused by systemic inflammation and body weight (especially abdominal obesity) should be fully

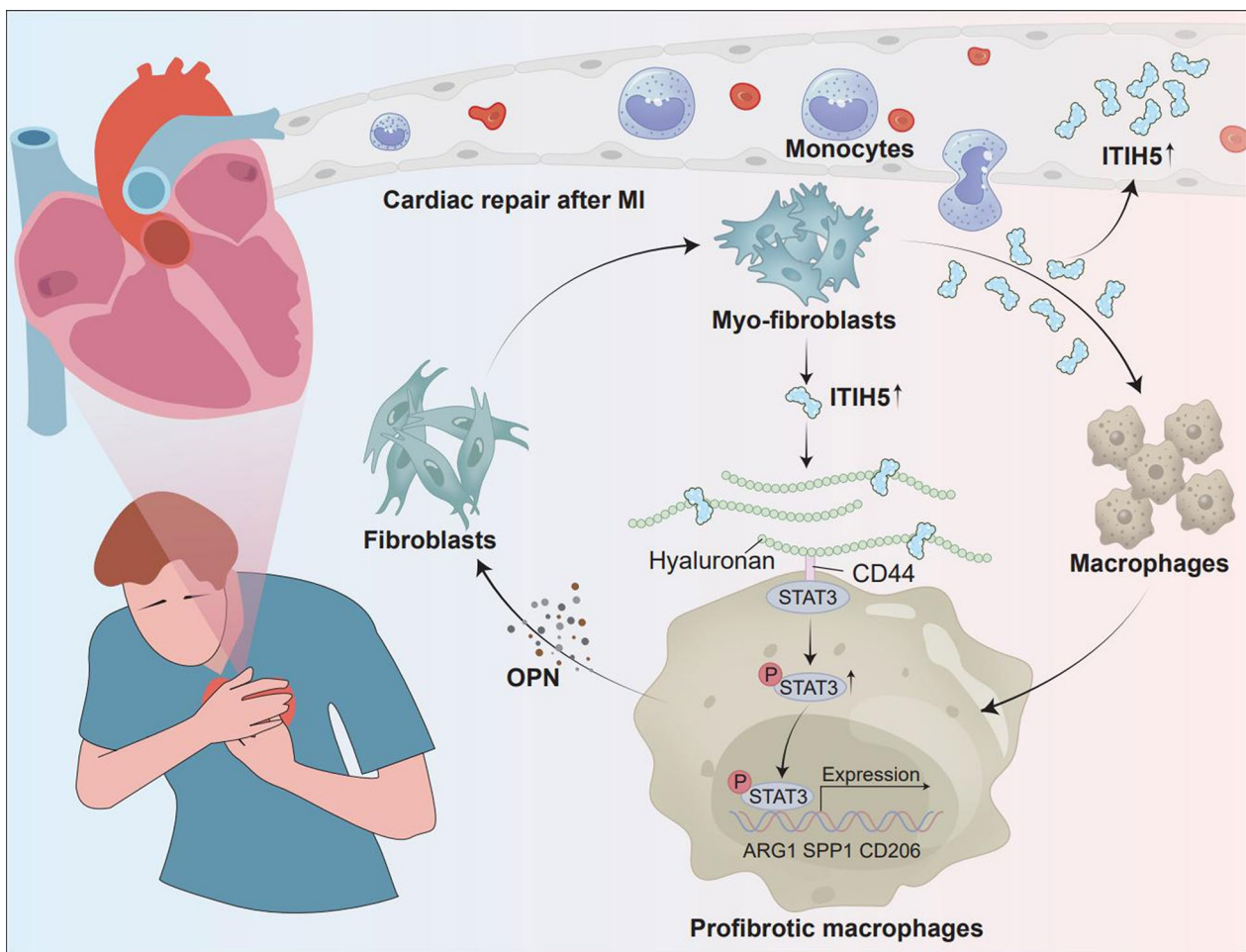


Fig. 8 Schematic illustration of ITIH5-mediated fibroblast–macrophage crosstalk exacerbates cardiac remodelling after MI. In myocardial tissue, ITIH5 expression is upregulated after MI and is localised to the ECM, regulating ECM-macrophage-fibroblast signalling network interaction thereby promoting macrophage profibrotic phenotype transformation, CFs activation and cardiac remodelling. In addition, highly expressed ITIH5 can be secreted into the peripheral blood and act as a biomarker in patients with ICM. In terms of mechanism of action, ITIH5 activates the CD44 receptors on the surface of the macrophage cell membrane in a hyaluronan-dependent manner and activates the macrophage STAT3 signalling pathway, promoting profibrotic phenotype transformation

considered when using peripheral blood ITIH5 levels to evaluate heart function.

In this study, we revealed that ITIH5, which is mainly expressed by CFs and distributed in the ECM as a secreted protein, was upregulated shortly after MI. Yang et al. also revealed that ITIH5 was mainly expressed in fibroblasts especially proinflammatory fibroblasts by scRNA sequencing [23]. This is consistent with the standard characteristic features of matricellular proteins [10]. It is worth noting that, similar to most matricellular proteins [10, 11], ITIH5 promoted fibrosis repair to a certain extent in the acute phase and reduced the risk of death due to malignant complications after MI. However, sustained upregulation of ITIH5 promoted reverse cardiac remodelling. Further studies on the regulatory

function of ITIH5 in fibroblasts reported that ITIH5 can promote proliferation, migration, and cell survival, consistent with the matricellular protein feature of promoting the semi-adhesion state that activates survival signals [9, 10]. However, in this study, we did not explore specific cell adhesion and cell survival signalling pathways. Based on these two features, we concluded that ITIH5 is a matricellular protein that regulates cardiac repair after MI to a certain extent. Nevertheless, it is unclear whether ITIH5 function is dependent on matricellular protein signatures, since truncated ITIH5, which has lost its N-terminal secretory sequence, can also regulate intracellular signalling to inhibit the hepatic metastasis of pancreatic ductal cell carcinoma [14]. In addition, ITIH5 can bind directly to the transcription factor KLF4 [15],

demonstrating its ability to regulate biological functions through non-ECM mechanisms.

In addition, we observed a significant inhibition of fibrosis in mice with ITIH5 knockdown; however, in vitro intervention of ITIH5 expression in CFs had no significant effect on collagen synthesis or myofibroblast transformation. Subsequent in vivo and in vitro experiments showed that ITIH5 has significant effects on macrophage infiltration, maturation, and phenotypic transformation, which may indirectly promote fibrosis. Traditional macrophages include classically activated (M1) and alternatively activated (M2) macrophages. The currently recognised cardiac macrophage clustering method mainly divides mouse cardiac macrophages into CCR2-MHCII^{low} TIMD4⁺ LYVE1⁺, CCR2-MHCII^{hi}, and CCR2⁺MHCII^{hi} [33, 34]. Although macrophages show strong pro-inflammatory features one day after MI, the macrophage expression repair phenotype seven days after MI does not fully express the markers of either M1 or M2 [3]. Compared to M1 macrophages, M2 macrophages have a stronger potential to promote fibrosis [35]. Accordingly, the newly defined macrophage subsets expressing TREM2, CD9, SPP1, GPNMB, FABP5, and CD63 are considered to have a strong potential to promote fibrosis [36]. Among these, TREM2 and SPP1, which are expressed by macrophages, have been widely reported to be closely related to fibrosis [37–41]. In addition, recruited macrophages also upregulate typical "M2" genes that are normally expressed in resident macrophages, such as CD206 and ARG1 [34]. Interestingly, CCR2⁺ macrophages having high expression signature of CD206, ARG1, TGF- β , PDGF and OPN, can significantly promote fibrotic remodelling after injury [38, 42]. In this study, we selected three signature genes, OPN, ARG1 and CD206, to characterize the ability of macrophages to promote fibrosis, and observed that ITIH5 promoted the expression levels of OPN, ARG1 and CD206 genes in macrophages. Concurrently, it was observed that the proportion of CCR2⁺ macrophages decreased in mice with ITIH5 knockdown in cardiac tissue confirming that ITIH5 can promote the recruitment of monocyte-derived macrophages after MI.

Recently, significant progress has been made in understanding the mechanism of fibroblast–macrophage interaction [43, 44]. In this study, we explored the ITIH5-mediated fibroblast–macrophage crosstalk using a co-culture system, which suggested that fibroblast–macrophage interactions further upregulated ITIH5 expression. ITIH5 overexpression in fibroblasts can also enhance macrophage profibrotic transformation and fibroblast activation, suggesting that ITIH5 can act as a positive feedback regulator of fibroblast–macrophage crosstalk.

Subsequent experiments showed that HA and its receptor CD44 play an important role in ITIH5-mediated regulation of macrophage function. HA provides an incompact ECM that promotes cell movement. Moreover, it transmits signals to cells via receptors such as CD44 and RHAMM. HA significantly affects immune response and fibroblast activation during ECM repair in a variety of cardiovascular diseases, including intimal hyperplasia, atherosclerosis, MI, and myocardial ischaemia–reperfusion injury [45–48]. In this study, we observed that the HA arrangement in the infarction area of mice with ITIH5 knockdown was more disordered than that in WT mice, and that 4-MU inhibited the macrophage profibrotic phenotype and fibroblast activation caused by ITIH5 overexpression. In an inflammatory environment, the polymer HA decomposes into low-molecular-weight HA fragments, which accumulate in inflammatory tissues. We observed that ITIH5 stabilised HA in the ECM. However, it is still unclear whether the HA stabilisation function of ITIH5 depends on bikunin-mediated heavy chain (HC) transfer because previous studies have revealed that ITIH5 and bikunin have different expression patterns in myocardial tissue [16]. Moreover, HC can undergo ECM modification independent of bikunin [49], and ITIH5 may bind to an unknown peptide or simply exist alone to stabilise HA in the ECM.

Similarly, this study confirmed that ITIH5 overexpression promotes its binding to CD44, and 4-MU treatment weakens this binding. Previous studies have reported that ITIHs promote adhesion of CD44-positive cells to HA [50]. Moreover, the function of macrophages and fibroblasts regulated by ITIH5 is closely related to CD44 because blocking CD44 significantly inhibits macrophage maturation and fibrotic phenotype transformation. However, it remains unclear whether ITIH5 can directly bind to CD44 or co-form an ECM complex with HA. Finally, activation of the STAT3 signalling pathway appears to be related to the binding ability of ITIH5 to CD44, as we revealed that blocking CD44 inhibits ITIH5 up-regulated STAT3 signalling activation. STAT3 is at the crossroads of multiple signalling pathways that regulate pro-inflammatory, anti-inflammatory, and macrophage-mediated tissue repair. STAT3 promotes macrophage M2 polarization in various cardiac disease models [51, 52]. In addition, STAT3 plays a role in macrophage-mediated cardiac repair after MI, mainly through IL10–STAT3–Gal3 signalling to promote CD206^{hi} macrophages to secrete OPN [38]. In addition, various membrane receptors are responsible for transmitting extracellular signals that activate the STAT3 pathway. In this study, ITIH5 enhanced the binding of CD44 to STAT3, which was reversed by blocking CD44. Furthermore, STAT3 inhibition could

reverse the macrophage profibrotic phenotype and fibroblast activation caused by ITIH5 overexpression in the co-culture system.

There are some limitations in our study. First, expanded clinical statistics including follow-up data need to be collected to evaluate the diagnostic and prognostic value of peripheral blood ITIH5 levels in patients with ICM. Second, ITIH5 knock-out or trans-genetic mice are needed to further illustrate the biological function of ITIH5 due to potential off-target effects or the specificity of the AAV used. Finally, detailed mechanism including how ITIH5 regulate the HA fuction and interact with CD44 receptor remains unknown and whether there are other extracellular matrix proteins that can also bind to ITIH5 to perform biological functions. However, our study highlights the crosstalk between CFs and macrophages during cardiac remodelling after MI in which ITIH5 plays a prominent role. Moreover, ITIH5, as a novel matricellular protein, could be applied in the biomaterials field to promote myocardial repair in acute phase after MI.

Conclusion

In summary, we demonstrated that ITIH5, which is markedly activated in ischaemic myocardial tissue, can be secreted into the peripheral blood as a blood biomarker in patients with ICM. Moreover, ITIH5 could regulate ECM–macrophage–fibroblast interactions and promote fibrotic remodelling after MI by promoting macrophage profibrotic phenotype transformation through binding to CD44 on the surface of the macrophage cell membrane through an HA-dependent pathway and then activating the STAT3 signalling pathway. Altogether, ITIH5 could be an ECM modulator for treating fibrotic remodelling after MI and other inflammation- and fibrosis-related cardiovascular diseases.

Abbreviations

AUC	Area under the curve
CF	Cardiac fibroblasts
DEGs	Differentially expressed genes
ECM	Extracellular matrix
ELISA	Enzyme-linked immunosorbent assay
FCM	Flow cytometry
GO	Gene ontology
GSEA	Gene set enrichment analysis
HA	Hyaluronan
HC	Heavy chain
ICM	Ischaemic cardiomyopathy
ITIH5	Inter- α trypsin inhibitor heavy chain 5
KEGG	Kyoto Encyclopedia of Genes and Genomes
LV	Left ventricle
LVEF	LV ejection fraction
LVFS	LV fractional shortening
LVIDd/LVIDs	LV internal dimensions at diastole/systole
MI	Myocardial infarction
NF	Non-failing

STAT3

Signal transduction and activator of transcription 3

Supplementary Information

The online version contains supplementary material available at <https://doi.org/10.1186/s12967-025-06244-5>.

Additional file 1.

Additional file 2.

Acknowledgements

We are grateful to all those who contributed to this study. We thank Haohao Lu for the excellent technical support in mice model construction and echocardiography examination and Wenxia Li and Hangjie Fu for the help with mice tail intravenous injection

Author contributions

YX, LX, YW, and YZ conceived/designed the study. YW, LM, ML, SZ, JH, XC, and LC acquired, analysed, and interpreted the data. JH, LC, XG, Hao C, and Huimin C provided essential research tools/samples. YW and LM drafted the manuscript. YX, LX, and YZ reviewed the manuscript. All authors read and approved the final manuscript.

Funding

This research was supported by Zhejiang Provincial Natural Science Foundation of China under Grant No.Y24H020026, the Zhejiang Provincial Medical and Health Science and Technology Program under Grant No. 2024KY179, and the Hangzhou Construction Fund of Key Medical Disciplines under Grant No. OO20200121.

Availability of data and materials

The original data contributing to the findings presented in the study are included in the article/supplementary figures. Further inquiries can be addressed to the corresponding author. The RNA-seq study were upload to GEO database (GSE273243). The relevant R code which used to process the merged dataset from GEO database were upload to github (github.com/roywu12/DATAPROCESS).

Declarations

Ethics approval and consent to participate

This study was approved by the Ethics Committee of Affiliated Hangzhou First People's Hospital, Zhejiang University School of Medicine and follows the Declaration of Helsinki. All the participants signed informed consent forms. Under the provisions of the Guide for the Care and Use of Laboratory Animals of Zhejiang Chinese Medical University and the Guide for the Care and Use of Laboratory Animals published by the US NIH (2011).

Consent for publication

Not applicable.

Competing interests

The authors declare that they have no competing interests.

Author details

¹Department of Cardiology, Affiliated Hangzhou First People's Hospital, Westlake University School of Medicine, Zhejiang 310006, China. ²Translational Medicine Research Center, Affiliated Hangzhou First People's Hospital, Westlake University School of Medicine, Zhejiang 310006, China. ³The Fourth School of Clinical Medicine, Zhejiang Chinese Medical University, Hangzhou 310053, China.

Received: 26 June 2024 Accepted: 11 February 2025

Published online: 24 February 2025

References

- Gerber Y, Weston SA, Enriquez-Sarano M, Manemann SM, Chamberlain AM, Jiang R, Roger VL. Atherosclerotic burden and heart failure after myocardial infarction. *JAMA Cardiol.* 2016;1:156–62.
- Bahit MC, Kochar A, Granger CB. Post-myocardial infarction heart failure. *JACC Heart Fail.* 2018;6:179–86.
- Yap J, Irei J, Lozano-Gerona J, Vanaprucks S, Bishop T, Boisvert WA. Macrophages in cardiac remodelling after myocardial infarction. *Nat Rev Cardiol.* 2023;20:373–85.
- Frangogiannis NG. Cardiac fibrosis. *Cardiovasc Res.* 2021;117:1450–88.
- Tallquist MD. Cardiac fibroblast diversity. *Annu Rev Physiol.* 2020;82:63–78.
- Bhattacharya M, Ramachandran P. Immunology of human fibrosis. *Nat Immunol.* 2023;24:1423–33.
- Rurik JG, Tombácz I, Yadegari A, Méndez Fernández PO, Shewale SV, Li L, Kimura T, Soliman OY, Papp TE, Tam YK, Mui BL, Albelda SM, Puré E, June CH, Aghajanian H, Weissman D, Parhiz H, Epstein JA. CART T cells produced in vivo to treat cardiac injury. *Science.* 2022;375:91–6.
- Aghajanian H, Kimura T, Rurik JG, Hancock AS, Leibowitz MS, Li L, Scholler J, Monslow J, Lo A, Han W, Wang T, Bedi K, Morley MP, Linares Saldana RA, Bolar NA, McDaid K, Assenmacher C-A, Smith CL, Wirth D, June CH, Margulies KB, Jain R, Puré E, Albelda SM, Epstein JA. Targeting cardiac fibrosis with engineered T cells. *Nature.* 2019;573:430–3.
- Bornstein P. Matricellular proteins: an overview. *J Cell Commun Signal.* 2009;3:163–5.
- Frangogiannis NG. Matricellular proteins in cardiac adaptation and disease. *Physiol Rev.* 2012;92:635–88.
- Dobaczewski M, Gonzalez-Quesada C, Frangogiannis NG. The extracellular matrix as a modulator of the inflammatory and reparative response following myocardial infarction. *J Mol Cell Cardiol.* 2010;48:504–11.
- Rose M, Kloten V, Noetzel E, Gola L, Ehling J, Heide T, Meurer SK, Gaiko-Shcherbak A, Sechi AS, Huth S, Weiskirchen R, Klaas O, Antonopoulos W, Lin Q, Wagner W, Veeck J, Gremse F, Steitz J, Knüchel R, Dahl E. ITIH5 mediates epigenetic reprogramming of breast cancer cells. *Mol Cancer.* 2017;16:44.
- Subramaniam K, Harihar S. An overview on the emerging role of the plasma protease inhibitor protein ITIH5 as a metastasis suppressor. *Cell Biochem Biophys.* 2024. <https://doi.org/10.1007/s12013-024-01227-z>.
- Young ED, Manley SJ, Beadnell TC, Shearin AE, Sasaki K, Zimmerman R, Kauffman E, Vivian CJ, Parasuram A, Iwakuma T, Grandgenett PM, Hollingsworth MA, O'Neil M, Welch DR. Suppression of pancreatic cancer liver metastasis by secretion-deficient ITIH5. *Br J Cancer.* 2021;124:166–75.
- Liu J, Cao F, Li X, Zhang L, Liu Z, Li X, Lin J, Han C. ITIH5, a p53-responsive gene, inhibits the growth and metastasis of melanoma cells by down-regulating the transcriptional activity of KLF4. *Cell Death Dis.* 2021;12:438.
- Anveden Å, Sjöholm K, Jacobson P, Palsdottir V, Walley AJ, Froguel P, Al-Daghri N, McTernan PG, Mejhert N, Arner P, Sjöström L, Carlsson LMS, Svensson P-A. ITIH-5 expression in human adipose tissue is increased in obesity. *Obesity.* 2012;20:708–14.
- Rönn T, Volkov P, Gillberg L, Kokosar M, Perfilov A, Jacobsen AL, Jørgensen SW, Brøns C, Jansson P-A, Eriksson K-F, Pedersen O, Hansen T, Groop L, Stener-Victorin E, Vaag A, Nilsson E, Ling C. Impact of age, BMI and HbA1c levels on the genome-wide DNA methylation and mRNA expression patterns in human adipose tissue and identification of epigenetic biomarkers in blood. *Hum Mol Genet.* 2015;24:3792–813.
- Rose M, Meurer SK, Kloten V, Weiskirchen R, Denecke B, Antonopoulos W, Deckert M, Knüchel R, Dahl E. ITIH5 induces a shift in TGF- β superfamily signaling involving Endoglin and reduces risk for breast cancer metastasis and tumor death. *Mol Carcinog.* 2018;57:167–81.
- Martin J, Midgley A, Meran S, Woods E, Bowen T, Phillips AO, Steadman R. Tumor necrosis factor-stimulated gene 6 (TSG-6)-mediated interactions with the inter- α -inhibitor heavy chain 5 facilitate tumor growth factor β 1 (TGF β 1)-dependent fibroblast to myofibroblast differentiation. *J Biol Chem.* 2016;291:13789–801.
- Huth S, Heise R, Vetter-Kauczok CS, Skazic K, Marquardt Y, Czaja K, Knüchel R, Merk HF, Dahl E, Baron JM. Inter- α -trypsin inhibitor heavy chain 5 (ITIH5) is overexpressed in inflammatory skin diseases and affects epidermal morphology in constitutive knockout mice and murine 3D skin models. *Exp Dermatol.* 2015;24:663–8.
- Huth S, Huth L, Marquardt Y, Fietkau K, Dahl E, Esser PR, Martin SF, Heise R, Merk HF, Baron JM. Inter- α -trypsin inhibitor heavy chain 5 (ITIH5) is a natural stabilizer of hyaluronan that modulates biological processes in the skin. *Skin Pharmacol Physiol.* 2020;33:198–206.
- Ruhl T, Sessler TM, Keimes JM, Beier JP, Villwock S, Rose M, Dahl E. ITIH5 inhibits proliferation, adipogenic differentiation, and secretion of inflammatory cytokines of human adipose stem cells—a new key in treating obesity? *FASEB J.* 2024;38:e23352.
- Yang L, Chen Y, Huang W. What links chronic kidney disease and ischemic cardiomyopathy? A comprehensive bioinformatic analysis utilizing bulk and single-cell RNA sequencing data with machine learning. *Life (Basel).* 2023;13(11):2215.
- Jin K, Gao S, Yang P, Guo R, Li D, Zhang Y, Lu X, Fan G, Fan X. Single-cell RNA sequencing reveals the temporal diversity and dynamics of cardiac immunity after myocardial infarction. *Small Methods.* 2022;6:e2100752.
- Ruiz-Villalba A, Romero JP, Hernández SC, Vilas-Zornoza A, Fortelny N, Castro-Labrador L, San Martín-Uríz P, Lorenzo-Vivas E, García-Olloqui P, Palacio M, Gavira JJ, Bastarrika G, Janssens S, Wu M, Iglesias E, Abizanda G, de Morentin XM, Lasaga M, Planell N, Bock C, Alignedani D, Meda G, Prudovsky I, Jin Y-R, Ryzhov S, Yin H, Pelacho B, Gomez-Cabrero D, Lindner V, Lara-Astiaso D, et al. Single-cell RNA sequencing analysis reveals a crucial role for CTHRC1 (collagen triple helix repeat containing 1) cardiac fibroblasts after myocardial infarction. *Circulation.* 2020;142:181–47.
- Carrara SC, Davila-Lezama A, Cabriel C, Berenschot EJW, Krol S, Gardeniers JGE, Izeddin I, Kolmar H, Susarrey-Arce A. 3D topographies promote macrophage M2d-Subset differentiation. *Materials Today Bio.* 2024;24:100897.
- Garnique ADMB, Machado-Santelli GM. Characterization of 3D NSCLC cell cultures with fibroblasts or macrophages for tumor microenvironment studies and chemotherapy screening. *Cells.* 2023;12:2790.
- Singh K, Gautam PK. Macrophage infiltration in 3D cancer spheroids to recapitulate the TME and unveil interactions within cancer cells and macrophages to modulate chemotherapeutic drug efficacy. *BMC Cancer.* 2023;23:1186.
- Huebener P, Abou-Khamis T, Zymek P, Bujak M, Ying X, Chatila K, Haudek S, Thakker G, Frangogiannis NG. CD44 is critically involved in infarct healing by regulating the inflammatory and fibrotic response. *J Immunol.* 2008;180:2625–33.
- Yang L-W, Qin D-Z, James E, McKallip RJ, Wang N-P, Zhang W-W, Zheng R-H, Han Q-H, Zhao Z-Q. CD44 deficiency in mice protects the heart against angiotensin II-induced cardiac fibrosis. *Shock.* 2019;51:372–80.
- Kim H, Cha J, Jang M, Kim P. Hyaluronic acid-based extracellular matrix triggers spontaneous M2-like polarity of monocyte/macrophage. *Biomater Sci.* 2019;7:2264–71.
- Simmonds SJ, Cuijpers I, Heymans S, Jones EAV. Cellular and molecular differences between HFpEF and HFrEF: a step ahead in an improved pathological understanding. *Cells.* 2020;9(1):242.
- Zaman R, Epelman S. Resident cardiac macrophages: heterogeneity and function in health and disease. *Immunity.* 2022;55:1549–63.
- Zaman R, Hamidzadeh H, Epelman S. Exploring cardiac macrophage heterogeneity in the healthy and diseased myocardium. *Curr Opin Immunol.* 2021;68:54–63.
- Kim Y, Nurakhayev S, Nurkesh A, Zharkinkov Z, Saparov A. Macrophage polarization in cardiac tissue repair following myocardial infarction. *IJMS.* 2021;22:2715.
- Fabre T, Barron AMS, Christensen SM, Asano S, Bound K, Lech MP, Wadsworth MH, Chen X, Wang C, Wang J, McMahon J, Schlerman F, White A, Kravarik KM, Fisher AJ, Borthwick LA, Hart KM, Henderson NC, Wynn TA, Dower K. Identification of a broadly fibrogenic macrophage subset induced by type 3 inflammation. *Sci Immunol.* 2023;8:eadd8945.
- Luo Q, Deng D, Li Y, Shi H, Zhao J, Qian Q, Wang W, Cai J, Yu W, Liu J. TREM2 insufficiency protects against pulmonary fibrosis by inhibiting M2 macrophage polarization. *Int Immunopharmacol.* 2023;118:110070.
- Shirakawa K, Endo J, Kataoka M, Katsumata Y, Yoshida N, Yamamoto T, Isobe S, Moriyama H, Goto S, Kitakata H, Hiraide T, Fukuda K, Sano M. IL (Interleukin)-10-STAT3-galectin-3 axis is essential for osteopontin-producing reparative macrophage polarization after myocardial infarction. *Circulation.* 2018;138:2021–35.
- Hulsmans M, Schloss MJ, Lee I-H, Bapat A, Iwamoto Y, Vinegoni C, Paccalet A, Yamazoe M, Grune J, Pabel S, Momin N, Seung H, Kumowski N, Pulous FE, Keller D, Beninc C, Green U, Lennerz JK, Mitchell RN, Lewis A, Casadei B, Iborra-Egea O, Bayes-Genis A, Sossalla S, Ong CS, Pierson RN, Aster JC, Rohde D, Wojtkiewicz GR, Weissleder R, et al. Recruited macrophages elicit atrial fibrillation. *Science.* 2023;381:231–9.

40. Collins AR, Schnee J, Wang W, Kim S, Fishbein MC, Bruemmer D, Law RE, Nicholas S, Ross RS, Hsueh WA. Osteopontin modulates angiotensin II-induced fibrosis in the intact murine heart. *J Am Coll Cardiol*. 2004;43:1698–705.
41. Seno H, Miyoshi H, Brown SL, Geske MJ, Colonna M, Stappenbeck TS. Efficient colonic mucosal wound repair requires Trem2 signaling. *Proc Natl Acad Sci USA*. 2009;106:256–61.
42. Clements M, Gershenovich M, Chaber C, Campos-Rivera J, Du P, Zhang M, Ledbetter S, Zuk A. Differential Ly6C expression after renal ischemia-reperfusion identifies unique macrophage populations. *J Am Soc Nephrol*. 2016;27:159–70.
43. Buechler MB, Fu W, Turley SJ. Fibroblast-macrophage reciprocal interactions in health, fibrosis, and cancer. *Immunity*. 2021;54:903–15.
44. Setten E, Castagna A, Nava-Sedeño JM, Weber J, Carriero R, Reppas A, Volk V, Schmitz J, Gwinner W, Hatzikirou H, Feuerhake F, Locati M. Understanding fibrosis pathogenesis via modeling macrophage-fibroblast interplay in immune-metabolic context. *Nat Commun*. 2022;13:6499.
45. Kiene LS, Homann S, Suvorova T, Rabausch B, Müller J, Kojda G, Kretschmer I, Twarock S, Dai G, Deenen R, Hartwig S, Lehr S, Köhrer K, Savani RC, Grandoch M, Fischer JW. Deletion of hyaluronan synthase 3 inhibits neointimal hyperplasia in mice. *Arterioscler Thromb Vasc Biol*. 2016;36:e9–16.
46. Homann S, Grandoch M, Kiene LS, Podsvyadek Y, Feldmann K, Rabausch B, Nagy N, Lehr S, Kretschmer I, Oberhuber A, Bollyky P, Fischer JW. Hyaluronan synthase 3 promotes plaque inflammation and atheroprotection. *Matrix Biol*. 2018;66:67–80.
47. Wang N, Liu C, Wang X, He T, Li L, Liang X, Wang L, Song L, Wei Y, Wu Q, Gong C. Hyaluronic acid oligosaccharides improve myocardial function reconstruction and angiogenesis against myocardial infarction by regulation of macrophages. *Theranostics*. 2019;9:1980–92.
48. Petz A, Grandoch M, Gorski DJ, Abrams M, Piroth M, Schneckmann R, Homann S, Müller J, Hartwig S, Lehr S, Yamaguchi Y, Wight TN, Gorresen S, Ding Z, Kötter S, Krüger M, Heinen A, Kelm M, Gödecke A, Flögel U, Fischer JW. Cardiac hyaluronan synthesis is critically involved in the cardiac macrophage response and promotes healing after ischemia reperfusion injury. *Circ Res*. 2019;124:1433–47.
49. Zhuo L, Kimata K. Structure and function of inter-alpha-trypsin inhibitor heavy chains. *Connect Tissue Res*. 2008;49:311–20.
50. Zhuo L, Kanamori A, Kannagi R, Itano N, Wu J, Hamaguchi M, Ishiguro N, Kimata K. SHAP potentiates the CD44-mediated leukocyte adhesion to the hyaluronan substratum. *J Biol Chem*. 2006;281:20303–14.
51. Lee T-M, Chang N-C, Lin S-Z. Dapagliflozin, a selective SGLT2 inhibitor, attenuated cardiac fibrosis by regulating the macrophage polarization via STAT3 signaling in infarcted rat hearts. *Free Radical Biol Med*. 2017;104:298–310.
52. Yang M, Zheng J, Miao Y, Wang Y, Cui W, Guo J, Qiu S, Han Y, Jia L, Li H, Cheng J, Du J. Serum-glucocorticoid regulated kinase 1 regulates alternatively activated macrophage polarization contributing to angiotensin II-induced inflammation and cardiac fibrosis. *ATVB*. 2012;32:1675–86.

Publisher's Note

Springer Nature remains neutral with regard to jurisdictional claims in published maps and institutional affiliations.